Thesis Proposal

An efficient optimization framework for gray-box PDE simulations and its application to a turbulent flow optimization problem

---

Han Chen
Ph.D Candidate

Massachusetts Institute of Technology
Department of Aeronautics & Astronautics

Aeronautics Computational Design Laboratory

Submitted on:

Thesis Committee: Qiqi Wang, Karen Willcox, Youssef Marzouk

Abstract

Gray-box simulations of partial differential equations (PDE) are present in many engineering applications. Unlike black-box simulations, we have some but limited insights of the PDEs in gray-box simulations. My thesis is interested in the optimization based on gray-box simulations, which is a common task in the engineering community. Conventional optimization practices treat the gray-box simulation as black-box. In many scenarios the gray-box simulation does not have adjoint implementations, so we can not compute sensitivities, specifically the gradients of the optimization's objective function, in an efficient way. When the dimension of optimization parameters is high, such conventional practices may require large amount of simulations which can be computational prohibitable.

My thesis proposes an efficient methodology for high-dimensional optimization problems by leveraging the limited insights about the gray-box simulations. My method constructs a physics-based surrogate, called twin model. In contrast to conventional PDE surrogates with fixed-physics, twin model has flexible physics so it can be trained by morphing itself to mimic the gray-box simulation. The training takes advantage of the space-time solution in time-dependent simulations, or space-solution in time-independent simulations. These solutions generally contain much more information about the gray-box simulation than the optimization's objective function alone. Because the twin model has the adjoint capability, the gradient of the objective function can be computed efficiently on twin model.

Optimization can be performed in a multi-fidelity framework using twin model, in which the twin model is low-fidelity, and the gray-box simulation is high-fidelity. My thesis proposes a provably convergent Bayesian optimization scheme that combines the evaluations of the gray-box objective function with the twin model gradient. For completeness we also extend the framework to deal with optimization problems with linear and nonlinear constraints.

We demonstrate our method in a turbulence flow simulation in a turbine airfoil trailing edge cooling problem. The gray-box simulation is an performed by OpenFOAM, a gray-box simulation with no adjoint capability, using large eddy simulation (LES). The twin model is a Reynolds-averaged Navier-Stokes (RANS) equations model with flexible Reynold stress modelling. We optimize a U-bend geometry to minimize the pressure loss across U-bend, constrained by minimum heat transfer.

Contents

1 Nomenclatures

2 Background

2.1 Optimization based on gray-box PDE simulation

Optimization problems is of great interest in the engineering community. We consider minimizaing an objective function:

$$J : \mathcal{C} \in \mathbb{R}^d \times [0, T] \to \mathbb{R}, \qquad c(t) \to J(c)\,,$$

where $c(t) \in \mathbb{R}^d$ for $\forall t$. $c(t)$ is the control variable to be optimized. In many cases, the objective function is an ouput of a PDE based, spatial-time simulation. These simulations are generally implementations of physics models, and can provide accurate predictions for the output quantity of interest. For illustration purpose, we will mostly use oil reservoir management and optimization problems. Though the method being developed is not restricted to reservoir problems.

In many cases, PDE-based simulations implement complex physics models and exotic solution techniques, and the physics models and implementations of solving the PDEs may not be accessible. For example, many industrial reservoir simulators are proprietary, such as *Eclipse* (Schlumberger), *VIP* (Halliburton), and *PSim* (ConocoPhillips). During an internship in ConocoPhillips, the author got a chance to look at *PSim*'s source code. It turns out to be a million-line, *Fortran77*, legacy code developed for decades. Therefore, even when the source code and the documentation are availble, it can still take tremendous amount of man power to access or modify the code. We call such simulations *black-box*, in the sense that the only duty of the simulation is to compute the objective function:

$$J = J(c; \kappa) \in \mathbb{R}\,, \tag{1}$$

where $\kappa \in \mathbb{R}^n$ are some pre-defined model properties (for example, porosity and permeability in oil reservoir simulation). c is the control variable to be optimized. The controls can also be not inside the PDE, but are parameters that defines the spatial domain of solving the PDE, for example, in airfoil optimizations. Fortunately, although it may be difficult to access the details of the simulation, it's often easy to write down the abstract form of the PDE. For example, many reservoir simulations can be written as [25]

$$\begin{aligned} \eta \frac{\partial u}{\partial t} + \nabla \cdot F(u, \kappa) &= q(u, c) \\ J &= \int_0^T \int_\Omega j(u, c)\ \mathrm{d}t\mathrm{d}\mathbf{x} \end{aligned} \tag{2}$$

generally with an impermeable boundary condition or other known boundary conditions. $u \in \mathbb{R}^n$ includes field quantities like pressure and saturation. $\eta, \kappa \in \mathbb{R}^n$ are geology properties like porosity and permeability. $q \in \mathbb{R}^n$ is a known or unknown model for the volumetric change of u. $F \in \mathbb{R}^n$ is an unknown flux term. And c is the time-space-dependent control variable, for example water injection rates. Another observation is, given c and κ, many simulators can output the discretized $u(t, x)$ in addition to J. We will call such simulations *gray-box* simulations [46] , in order to distinguish *black-box* simulations where the underlying PDE, the boundary conditions, and $u(t, x)$ are unknown. The opposite of black-box simulation is *open-box* simulation.

Thanks to the complexity of physics models and large time-space scale involved, running a PDE-based simulation can be computationally expensive. In addition, optimization problems may entail a large number of PDE simulations. To give insights to this issue, let's suppose the time domain $[0, T]$ is discretized into m points, then we need to search in a $\mathbb{R}^{d \times m}$ space for the optimum. When $d \times m$ is larger, more simulations may be invoked due to the larger search space. Therefore optimization based on PDE-simulations can be costly.

We will restrict our attention to optimization based on gray-box simulations with a high-dimensional control space.

2.2 Problem setup

We consider the PDE governing the gray-box simulation to take the form:

$$\frac{\partial \eta_i u_i(t,x)}{\partial t} + \nabla \cdot F_i(\mathcal{D}u, \kappa) = q_i(u, c(t,x))\,, \qquad i = 1, \cdots, n\,, \tag{3}$$

where $x \in \Omega \subseteq \mathbb{R}^n$ is the spatial coordinate. $\partial\Omega$ is the boundary. $t \in [0, T]$ is time. The boundary condition is known. $F_i(\cdot,\cdot)$'s are the unknown flux functions. $u = \{u_1, \cdots, u_n\}$.
$\mathcal{D}u = \left\{u_1, \nabla u_1, \cdots, \nabla^{i_1} u_1; \cdots; u_n, \nabla u_n, \cdots, \nabla^{i_n} u_n\right\}$, where ∇^j indicates the jth order spatial derivative tensor. We assume $i_1, \cdots, i_n$, i.e. the maximum order of derivatives, are known. $\eta_i = \eta_i(x)$, $\kappa = \kappa(x)$ are problem dependent spatial variables, and is assumed known. $c(t,x)$ is a spatial-time-dependent control variable. $q_i(\cdot,\cdot)$'s are known or unknown functions. The discretized space-time solution of Eqn(3) given by a simulator is written as $\hat{u}(t_i, \mathbf{x}_i; c)\,,\ i = 1, \cdots, N$.

The objective function is defined by

$$J = \int_0^T \int_\Omega j(u,c)\mathrm{d}\mathbf{x}\mathrm{d}t \tag{4}$$

Notice j can depend explicitly on c, while u depends implicitly on c.

Let's consider a concrete example. Consider a simulator modeling two phase flow in porous media. One of the simplest yet classical model for two-phase porous media flow is the Buckley-Leverett model [28]. It models the displacement process of two-phase flow due to capillary pressure and Darcy's law [29]. The PDE, Buckley-Leverett equation, is

$$\frac{\partial u}{\partial t} + \frac{\partial}{\partial x}\left(\frac{u^2}{1 + A(1-u)^2}\right) = c\,, \tag{5}$$

where $u = u(t,x)$, $0 \le u \le 1$, is the saturation of phase I (e.g. water), and $1-u$ is the saturation of phase II (e.g. oil). $A > 0$ is a parameter dependent on the physical property of the two phases. $c = c(t,x)$ is the control variable. $c > 0$ models the injection of phase I replacing phase II; and $c < 0$ vice versa.

Suppose we want to control the flow through c, such that the saturation at $t = T$ is close to a target saturation $u^*(x)$. We introduce an L_2 penalty to the objective function for regularization [30]. The regularization can be interpreted as the cost of control. Hereby the objective function

$$\begin{aligned} J &= \int_x |u(T,x) - u^*(x)|^2\,\mathrm{d}x + \eta \int_t \int_x c^2(t,x)\mathrm{d}x\mathrm{d}t \\ &= \int_t \int_x |u(t,x) - u^*(x)|^2\,\delta_T(t) + \eta c^2(t,x)\mathrm{d}x\mathrm{d}t\,, \end{aligned} \tag{6}$$

where $\eta > 0$ models the magnitude of the regularization, and $\delta.(\cdot)$ indicates the Direc delta function. The optimization problem is

$$c^* = \arg\min_{c \in \mathcal{C}} J \tag{7}$$

where $\mathcal{C}$ is the L_2-function Hilbert space. Notice the optimization is unconstraint.

2.3 Gradient-free and gradient-based optimization

Existing methods for optimization can be classed into two categories: using gradient information (gradient-based optimization) and not using gradient information (gradient-free optimization) [1, 34]. Gradient-free optimization methods require only the availability of objective function values but not derivative information[19]. Because of its mild requirement of the simulation, gradient-free optimization methods are suitable for optimization problems based on *black-box* simulations, and enjoy a wide range of applicability. However, when the dimension of the search space $d \times m$ increases, these methods generally suffer

from the *curse of dimensionality*. The term *curse of dimensionality* refers to problems caused by the rapid increase in the search volume associated with adding extra dimension in the search space[20]. It's not uncommon to encounter hundreds of dimensions in real life engineering problems, limiting the applicability of gradient-free optimization in these cases. Several strategies have been proposed to address this challenge [45], such as dimensional reduction [47], system decomposition [48], and variable selection [49]. However, these methods generally assumes special structures of the system to work properly [45].

In contrast, gradient-based optimizations use gradient information to locate the local optimum. A well-known example is the quasi Newton's methods [21]. Generally gradient-based methods require less number of simulations to converge than gradient-free methods, and are more efficient at finding local optimum for high-dimensional problems. In addition of requiring $J(c)$ from the simulation, these methods also require $\frac{\partial J}{\partial c}$, the sensitivity. Adjoint methods are efficient methods for sensitivity analysis[23] for open-box models. Continuous adjoint method develops the continuous adjoint equations from the continuous PDE of the simulation through Lagrange multiplier; and it requires the PDE of the simulation. Discrete adjoint methods applys variational methods directly to the discretized PDE; and it requires the discretized PDE (i.e. the numerical implementation) of the simulation. Thus, adjoint methods can not be applied to compute the sensitivity of a black-box simulation. Another popular method to compute sensitivity is automatic differentiation (AD)[24]. AD exploits the fact that every computer program can be broken down into a sequence of elementary arithmetic operations and elementary functions. By applying the chain rule repeatedly to these operations, derivatives of arbitrary order can be computed automatically. Because AD requires the accessibility of every elementary operation during a simulation, it can not be used to compute the sensitivity of a black-box simulation either.

To sum up, gradient-free optimization methods are suitable for gray-box simulations, but suffer from the curse of dimensionality; gradient-based optimization methods are more efficient for high-dimensional problems, but are not suitable for gray-box simulation. This dilemma motivates the development of a new optimization strategy. The objective of my thesis is to design a new optimization strategy that: 1. not require $\frac{dJ}{dc}$ from the gray-box simulation, and 2. be suitable for high-dimensional problems.

2.4 Proposal outline

In the following chapters we will develop a new optimization strategy to address this problem. The first step of the new strategy is to construct a surrogate of $\frac{dJ}{dc}$ (gradient surrogate) using only the input and output of the gray-box simulation. We will develop such a surrogate in section 4 and section 4.8: section 4 discusses the surrogate with fixed structure; whereas section 4.8 discusses the surrogate with an adaptive structure. The next step of the strategy is to optimize $J(c)$ using both the samplings of $J(c)$ and the samplings of the gradient surrogate. In section 5.2 we will model the objective function and the surrogate as realizations of stochastic processes, hereby unify the samplings of $J(c)$ and the gradient surrogate inside a Bayesian framework. In section 5.3 we will apply an Bayesian optimization method, the expected improvement algorithm [3], to the unified Bayesian modelling, and discuss its convergence. In section **??** we will summarize the algorithm. A numerical example of water-oil displacement process will be shown in chapter 5.6 to illustrate the advantage of the new strategy.

3 Problem statement / Thesis objective / Expected contribution / Timeline

3.1 Problem statement

There are many turbulence models ranging from low to high in terms of complexity and fidelity. Turbulence flow optimization generally considers objective functions of time averaged flow field. RANS model simulates a time averaged flow field directly, but the result can be inaccurate. Optimization based solely on high-fidelity simulations (e.g. LES, DNS) yields the most credible result. However, such optimization is computationally challenging. The challenge is two-folded: Firstly, these simulations generally require a tremendous amount of spatial-time discretization grid for sufficient resolution, and each objective function evaluation can be both lengthy in time and costly in computational resources. Secondly, these high-fidelity simulators generally do not have adjoint capability; so estimations of the gradient, a key to efficient optimization, is difficult to obtain especially for high dimensional design space.

To alleviate this problem, multifidelity optimization have been applied to turbulence optimization for many years. Low fidelity models such as RANS are not only cheaper to evaluate, but also easier to implement the adjoint and evaluate the gradient. However, low-fidelity models may not be good representation of high-fidelity models, thus limiting computational savings.

3.2 Thesis objective

1. Develop a method for inferring a surrogate PDE from the space time solution of an unknown PDE simulation.
2. Assess how much computational saving can be achieved by using the high-fidelity model's space time solution in a return bend numerical testcase.

3.3 Expected contribution

1. Enable adjoint gradient computation even if the governing PDE is not available.
2. Demonstrate that efficient gradient-based optimization is possible, even if the underlying simulator does not implement an adjoint.
3. Demonstrate my method's superiority in a high-fidelity turbulent flow optimization with a high-dimensional design space.

3.4 Timeline

- Apr: Proposal defense documentation and slides
- May: Defend proposal. Demonstrate the complete algorithm on a the 1D Buckley-Leverett example.
- Jun: Setup an LES solver for the return bend testcase in OpenFoam, write a RANS solver with adjoint for the return bend.
- Jul-Oct: Implement the proposed method on the return bend example.
- Aug-Nov: Thesis writing
- Jan: Defense

4 Twin model

4.1 Review of surrogate methods

As mentioned in chapter 2, straightforward optimization of the objective function, i.e. by applying optimization routine directly to $J(c)$, is not always practical. A well-studied topic to address this problem is *surrogate-based optimization* [34, 35]. It is proposed to achieve optimization at reduced computational cost [36]. A *surrogate* is a reasonably accurate representation of the high-fidelity model $J(c)$. In the following context we will call the high-fidelity $J(c)$ the *primal model*, and write the surrogate model as $\tilde{J}(c)$. In surrogate-based optimization, the optimization of the primal model is replaced by iteratively updating and re-optimizing the surrogate. The design point generated by optimizing the surrogate is verified by evaluating the primal model. The primal model evaluation is then used to update the surrogate. Surrogate-based optimization generally proceeds in this prediction-correction manner until termination.

Surrogate-based optimization methods can be distinguished by how the surrogate is constructed. Surrogate construction techniques can be categorized into *physics-based surrogate* and *functional surrogate* [34]. Similar to the primal model, physics-based surrogate simulates the underlying physics. The surrogate is still a representation of the underlying system's physics, but has lower fidelity and is cheaper to evaluate: generally because it uses simplified physics [38, 36] and/or uses coarse discretization [39]. A functional surrogate, on the other hand, are constructed using only the sample values of $J(c)$ obtained from the primal model (and gradient of $J(c)$ if the primal model can also evaluate the gradient [40]). Functional surrogate does not require previous knowledge of the physics system of interest. Popular functional surrogate techniques include polynomial approximation [41], Kriging [42], and artificial neural network [43], etc.

Generally, physics-based surrogates are more expensive to evaluate but more accurate, mainly because they already embed some knowledge of the system's physics. However, physics-based surrogates are dedicated to the specific systems of interest. The construction of physics-based surrogates often require expert insights and significant coding manpower [34]. Functional surrogates, on the other hand, are generic to a wide class of problems. The price paid is they may require considerable amount of primal model evaluation to achieve the same accuracy as physics-based surrogates.

Designing a good physics-based surrogate requires expert insight (e.g. the choice of empirical formulas or the negligence of unimportant physics components), thus limits its applicability. Another drawback lies in the fact their underlying physics is fixed. Generally these models are only good approximation of the primal model within a certain range of physics settings. In optimization, however, design parameters move at each iteration. A low-fidelity model may gradually lose its accuracy as the design parameters moves away from the surrogate's applicable region. For example, the thin airfoil theory is only valid before stall. If one is to optimize the attack angle, the thin airfoil models may no longer provide good estimation of the primal model when the attack angle increases [50]. Another example is from turbulent modelling. Some simplified fluid models are derived under the assumption of low Reynolds number [52], while some are derived under high Reynolds number [51]. If one is to optimize the flow speed, the quality of using the simplified fluid models as surrogate can be questionable.

To sum up, physics-based surrogates have two drawbacks: 1. They require expert knowledge for construction. 2. Their physics are fixed offline and may not always give good approximations during optimization.

4.2 Envision of twin model

To alleviate these drawbacks, we can *correct* the surrogate's objective function iteratively online to improve its accuracy. One method is *Bayesian model calibration* [7, 2]. This approach models the (global) error, $J(c) - \tilde{J}(c)$, as a deterministic but unknown realization of a stochastic process. Hereby infer the error at unsampled c via a Bayesian framework, using existing samples of $J(c)$ and $\tilde{J}(c)$. The inferred error is then added to $\tilde{J}(c)$ to provide a corrected surrogate. Another method is *multi-fidelity trust-region method*, i.e. to bound the search step inside a *trust region* during each optimization iteration [14].

Within each trust region, the surrogate can be corrected to guarantee good (local) estimation of the primal model (e.g. satisfying the *fully-linear* property [13]), thus guaranteeing convergence.

These research efforts (Bayesian model calibration, multi-fidelity trust-region methods, etc) can be viewed as overlaying the existing surrogate model with an additional *functional* surrogate for correction. In order for the correction to improve the existing surrogate to a desirable accuracy, a large number of primal model evaluations may be required. As we mentioned earlier, this is a common problem suffered by functional surrogate. In the mean time, the *physics* of the physics-based surrogate is still fixed offline before the optimization. Can we use primal model samplings to directly correct the physics of the surrogate? Bearing this question at mind, we propose *twin model*: a physics-based surrogate model with flexible physics.

My envision is: the physics of twin model should have a learning ability. In other words, twin model should be able to morph its representation of the underlying system's physics on-the-fly, so as to mimic the behavior of the primal model for a wider range of physics settings. Besides, according to our gray-box assumptions in chapter 2, the learning process should treat the primal model non-intrusively. In other words, the only knowledges available in the learning process are sampled $J(c)$'s and corresponding space-time solutions $u(t, x; c)$'s of the primal model. Finally, the learning process should be disciplined and automated. Once the optimization started, no human intervention would be required to adjust the physics of the twin model.

Is the envision feasible? Consider a general dynamical system

$$\dot{u} = \mathcal{L}(u)\,, \tag{8}$$

where $u = \{u_1, \cdots, u_n\}$, $u_i = u_i(t, x)$, $i = 1, \cdots, n$, $x \in \mathbb{R}^n$. $\mathcal{L}$ is a differential operator known as the Hamiltonian of the system [54]. Suppose an observer can take snapshots of u at any t. It has been shown that inferring $\mathcal{L}$ from the snapshots is an intractable problem, no matter how many snapshots are observed [53]. Although Eqn(8) offers the most general description of the primal model, we may not be able to construct a practical twin model just based on Eqn(8).

However, inferring the differential operator $\mathcal{L}$ is not necessary. As discussed in chapter 2, the PDE that governs the primal model can already be written as Eqn(3). Therefore, the problem of adjusting twin model's physics reduces to the problem of adjusting a set of functionals $F_i(\mathcal{D}u, \kappa)$, for $i = 1, \cdots, n$. In addition, we can use the discretized space-time solution $\hat{u}(t_i, \mathbf{x}_i; c)$, provided by the primal model, to adjust the physics of twin model. $\hat{u}(t_i, \mathbf{x}_i; c)$ is a by-product of evaluating $J(c)$, but provides more information than $J(c)$ about the underlying system's physics [1]. Finally, as we write the twin model in a conservative form, the implementation of twin model can be guaranteed to conform to conservation laws using appropriate numerical schemes such as finite volume methods [55].

To sum up, we aim at inferring the functional F_i's in Eqn(3) using the space-time solutions $\hat{u}$ of the primal model.

4.3 Review of system identification

The inference problem is a *system identification* problem. System identification is a method that builds mathematical models of a dynamical system from its measured data [56]. Depending on the how the system is modelled, system identification can be classified into *linear system identification* and *nonlinear system identification*. Linear system identification assumes a linear relationship between the system inputs $\mathbf{x}(t)$ and output $y(t)$:

$$y(t) = h_0 + \sum_{i=1}^{n} \int_0^t h_i(\tau) x_i(t - \tau)\, d\tau \tag{9}$$

The advantage is a linear model can be determined solely by its impulse response function. Clearly, the twin model is generally nonlinear and may not be modelled well by a linear system. Nonlinear system

identification does not assume this linearity, thus is more generic [5]. We will restrict our attention to nonlinear system identification.

Well-known models for nonlinear system identification include [5]: *piecewise linear models*, *block-structured models*, *Volterra models*, and *NARMAX* models. A piecewise linear model develops a series of locally linear approximations to the system. In our problem, this model would adopt a piecewise linear representation of F_i's and q_i's. This approach can utilize the wealth of knowledge obtained from the research in linear systems. But a drawback is the difficulty to partition the parameter domain, because the estimation of piecewise model can not be easily separated from the task of finding the domain for each sub-model [57].

Block-structured models are described by connections of groups of linear and nonlinear models [5]. For example, Hammerstein model applies a nonlinear scaling of the input before transmitting it to a linear dynamic model described by Eqn(9). Wienner model, on the other hand, applies the nonlinear scaling after the dynamic model.

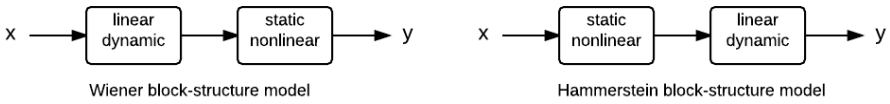

Figure 1: block structure model

These models became popular after theoretical results showing a nonlinear scaling operation preserves the cross variance of Gaussian stochastic signals [60]. Another type of block-structured models are feedback linear models, in which the output of the linear dynamic model is feed to its input [61].

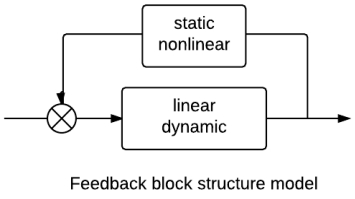

Figure 2: feedback model

However, almost all these methods rely on previous knowledge that the system under study has a specific structure [5]. Besides, most researches on block-structured models focus on SISO, MISO, and MIMO systems, instead of PDE systems. They directly model the transformation from the system input to the system output, failing to take advantage of the PDE form expressed by Eqn(3). Indeed, block-structured models may overly restrict the form of the model. We would prefer a more general description of the model.

Volterra models, a.k.a. Volterra series models, use polynomials to represent the system. It is similar to a Taylor series but has a memory effect [58, 59]. If we think of Taylor series as a functional that applies to a snapshot of $u(x,t)$ for a fixed t, then the Volterra series can be thought as a functional that applies to the whole history of $u(x,t)$ [5]. We call a Volterra model of kth order if the polynomial is of kth order. For example, if $F = F(x(t))$, then an mth order Volterra model on $t \in [0,T]$ would approximate F as

$$\begin{aligned} F &\approx h_0 + \sum_{k=1}^{m} H_k x(t) \\ H_k x(t) &= \int_{\tau_1=0}^{T} \cdots \int_{\tau_k=0}^{T} h_k(\tau_1, \cdots, \tau_k) \prod_{j=1}^{k} x(t-\tau_j) d\tau_j \end{aligned} \tag{10}$$

More generally, for $F = F(x_1(t), \cdots, x_n(t))$, an mth order Volterra model would be [58]

$$F \approx h_0 + \sum_{p=1}^{m} H_p \mathbf{x}(t)$$

$$H_p\mathbf{x}(t) = \sum_{\substack{k_1 \geq 0, \cdots, k_n \geq 0 \\ k_1 + \cdots + k_n = p}} \int_{\tau_{j_1}} \cdots \int_{\tau_{j_n}} \prod_{j_1=1}^{k_1} \cdots \prod_{j_n=1}^{k_n} h_{k_1,\cdots,k_n}(\tau_{j_1}, \cdots, \tau_{j_n}) x_1(t-\tau_{j_1}) d\tau_{j_1} \cdots x_n(t-\tau_{j_n}) d\tau_{j_n} \tag{11}$$

A special case of Volterra model is a *memoryless* polynomial expansion, written as

$$H_p\mathbf{x}(t) = \sum_{\substack{k_1 \geq 0, \cdots, k_n \geq 0 \\ k_1 + \cdots + k_n = p}} h_{k_1,\cdots,k_n} x_1^{k_1}(t) \cdots x_n^{k_n}(t) \tag{12}$$

As discussed in section 2.2, our unknown flux function F_i only depends on $\mathcal{D}u = \left\{u_1, \nabla u_1, \cdots, \nabla^{i_1} u_1; \cdots; u_n, \nabla u_n, \cdots, \nabla^{i_n} u_n\right\}$, rather than depending on the time history of u. Therefore Eqn(12) suffices to describe the unknown flux.

NARMAX models (nonlinear autoregressive moving average models with exogeneous parameters), introduced in [62], provides a more general model description. Initially it was invented to model a *discrete* SISO system with exogeneous inputs $\mathbf{u}$ and output noise $\mathbf{e}$:

$$y(t) = F[y(t-1), y(t-2), \cdots, y(t-n_y), u(t-1), u(t-2), \cdots, u(t-n_u), e(t-1), e(t-2), \cdots, e(t-n_e)] + e(t) \tag{13}$$

Hereby NARMAX' name. While NARMAX started as the name of a model, it has now developed into a philosophy of nonlinear system identification. The philosophy consists of the following steps to identify a model [5]:

- *Model representation*: Represent F by a library of terms
- *Structure detection*: Remove unnecessary terms in the expansion
- *Parameter estimation*: Fit the term coefficients
- *Model validation*: Check if the model's error is predictable

The first step is to expand the functional form F by a *linear* combination of a library of *basis* terms; for example, using Volterra series models, wavelet decomposition [64], neural networks [63], etc. The choice of the library is up to the user's choice. However, a naive proceeding to fitting the coefficients of all the terms in the library can be computationally intractable. Often there are only a few terms in the library that are important in the model. So the next step is to detect those terms. NARMAX proceeds this step by first selecting the most important term, then the next most important terms, and so on, until a termination criterion is met. We'll investigate the structure detection step in greater detail in section 4.8. After the structure detection, NARMAX estimates the coefficients of the terms, for example using a mean square error approach, so the output of the identified model and the underlying system match on the sampled inputs. Finally, the model is validated to check if the identified model is adequate, for example, if there is anything predictable left in the model output's error [65]. Unless the model is determined adequate, the term library will be enlarged and the previous procedures will be conducted again. We'll discuss the model validation step in section **??**.

We will adopt the NARMAX philosophy to identify the twin model because of two considerations. Firstly, NARMAX is generic. It does not pose any limitation on the model representation library beforehand. Secondly, NARMAX is parsimonious. It attempts to find the simplest model structure before fitting the term coefficients. In my thesis, we will expand the functionals F_i's in Eqn(3) by a library of terms. The choices of the library will be explored. Then we will use NARMAX philosophy to fit the F_i's. Chapter 4 will discuss fitting the twin model without the structure detection step, i.e. twin model with fixed structure. Chapter 4.8 will focus on the structure detection.

4.4 Formulation of twin model with fixed structure

In the parameter estimation step, we need a *criterion* to determine if the twin model matches the primal model. Given the same inputs (controls c, initial conditions, boundary conditions, and exogenous inputs κ and η), suppose the space-time solution generated by the primal model is u. An ideal twin model should provide a space-time solution $\tilde{u}$ such that $J(\tilde{u}, c)$ is a good estimate of $J(u, c)$. Therefore a straightforward criterion is to minimize the difference of the objective functions

$$|J(\tilde{u}, c) - J(u, c)| \tag{14}$$

However, computing J effectively compresses the space-time solution into just one number, where lots of information contained in u would be lost [1]. To take advantage of the space-time solution, we consider the minimization of

$$\frac{1}{T}\int_{t=0}^{T}\int_{\mathbf{x}\in\Omega} w^2(t, \mathbf{x}, u, \tilde{u})(\tilde{u} - u)^2 \, dtd\mathbf{x}\,, \tag{15}$$

where $w^2 > 0$ is a weight possibly depending on t, $\mathbf{x}$, u, and $\tilde{u}$. Eqn(15)$\to 0$ provides a sufficient condition for Eqn(14) $\to 0$, but the reverse is not true. We will delay the discussion of w to section **??**. Right now we assume $w \equiv 1$ for simplicity. Notice the square on $\tilde{u} - u$: it is the most popular norm and is differentiable. The reason of using a differentiable expression will be discussed soon in this chapter.

The space-time solution is discretized rather than continuous. If the twin model and the primal model use the same space-time grid, then Eqn(15) can be approximated by

$$\frac{1}{T}\sum_{i=1}^{N}\sum_{k=1}^{T}(\tilde{u}_{ik} - u_{ik})^2 \, \Delta t_k \, |\Delta \mathbf{x}_i| \;, \tag{16}$$

where $|\Delta \mathbf{x}_i|$ indicates the size of the grid. If the grids are different, then a mapping P from u to $\tilde{u}$ is required. In this case, Eqn(16) would translate to

$$\frac{1}{T}\sum_{i=1}^{N}\sum_{k=1}^{T}(\tilde{u}_{ik} - P(u)_{ik})^2 \, \Delta t_k \, |\Delta \mathbf{x}_i| \;, \tag{17}$$

Right now, we assume the grids are the same for simplicity. In addition, we assume the right hand side q_s in the twin model is known. Extension to unknown q_s will be discussed later.

To sum up, the problem of constructing a twin model (with fixed structure) is converted to the following problem:

Solve

$$\xi^* = \arg\min_{\xi} L(\tilde{u}(\xi)) = \arg\min_{\xi}\left\{\frac{1}{T}\sum_{i=1}^{N}\sum_{k=1}^{T}(\tilde{u}_{ik} - u_{ik})^2 \, \Delta t_k \, |\Delta \mathbf{x}_i| + \lambda\|\xi\|^2\right\}, \tag{18}$$

where u is the discretized space-time solution of the primal model, and $\tilde{u}$ is the discretized space-time solution of

$$\frac{\partial \eta_s \tilde{u}_s(t, x)}{\partial t} + \nabla \cdot \left\{\sum_{k=1}^{m_s} \xi_{sk} g_{sk}(\mathcal{D}\tilde{u}, \kappa)\right\} = q_s(\tilde{u}, c(t, x))\,, \qquad s = 1, \cdots, n\,, \tag{19}$$

g_{sk}, $k = 1 \cdots m_s$ are the library of basis functions for F_s. ξ's are the coefficients for the basis functions. $\lambda\|\xi\|^2$ is the regularization with $\lambda > 0$. $\|\cdot\|$ is the L_2 vector norm. The grids of the primal model solver and the twin model solver are assumed the same. Also, the primal model and the twin model use the same control, initial condition, boundary condition, and exogeneous parameters η and κ.

Although the twin model method was developed for fitting a time-dependent PDE, the idea can be extended to time-independent PDE as well. Twin models for time-independent PDEs can be viewed as a special case for time-dependent PDEs. Consider solving a time-independent PDE with an iterative solution method with pseudo time marching (assume stability is satisfied), then we are only interested in matching the solutions *at the very last pseudo timestep*. The formulation is given below

Solve

$$\xi^* = \arg\min_{\xi} L(\tilde{u}(\xi)) = \arg\min_{\xi} \left\{ \sum_{i=1}^{N} \left(\tilde{u}_{ik} - u_{ik}\right)^2 |\Delta \mathbf{x}_i| + \lambda \|\xi\|^2 \right\}, \tag{20}$$

where u is the discretized spatial solution of the primal model, and $\tilde{u}$ is the discretized spatial solution of

$$\nabla \cdot \left\{ \sum_{k=1}^{m_s} \xi_{sk} g_{sk}(\mathcal{D}\tilde{u}, \kappa) \right\} = q_s(\tilde{u}, c(x)), \qquad s = 1, \cdots, n, \tag{21}$$

g_{sk}, $k = 1 \cdots m_s$ are the library of basis functions for F_s. ξ's are the coefficients for the basis functions. $\lambda\|\xi\|^2$ is the regularization with $\lambda > 0$. $\|\cdot\|$ is the L_2 vector norm. The grids of the primal model solver and the twin model solver are assumed the same. Also, the primal model and the twin model use the same control, boundary condition, and exogeneous parameters κ.

4.5 Adjoint-based parameter estimation of twin model

Similar to optimizing J, constructing a twin model is another optimization problem. However, the latter problem is easier to solve because the twin model, Eqn(19), is an open-box model. As mentioned in chapter 2, open-box models admit efficient gradient-driven optimization, where the gradient $\frac{dL}{d\xi}$ can be computed by adjoint method [22, 23]. To obtain the gradient, we first linearize L in Eqn(18),

$$\delta L = \left(\frac{dL}{d\tilde{u}}\right)^T \delta\tilde{u} \tag{22}$$

Then we linearize the residual $\tilde{R}(\tilde{u}, \xi)$ of Eqn(19),

$$\frac{\partial \tilde{R}}{\partial \tilde{u}} \delta\tilde{u} + \frac{\partial \tilde{R}}{\partial \xi} \delta\xi = 0 \tag{23}$$

Introduce a Lagrange multiplier λ, a.k.a. *adjoint state*, we have

$$\begin{aligned} \delta L &= \left(\frac{dL}{d\tilde{u}}\right)^T \delta\tilde{u} - \lambda^T \left(\frac{\partial \tilde{R}}{\partial \tilde{u}} \delta\tilde{u} + \frac{\partial \tilde{R}}{\partial \xi} \delta\xi \right) \\ &= -\left(\lambda^T \frac{\partial \tilde{R}}{\partial \xi}\right) \delta\xi + \left(\left(\frac{dL}{d\tilde{u}}\right)^T - \lambda^T \frac{\partial \tilde{R}}{\partial \tilde{u}} \right) \delta\tilde{u} \end{aligned} \tag{24}$$

Therefore, the adjoint state satisfies the *adjoint equation*

$$\left(\frac{\partial \tilde{R}}{\partial \tilde{u}}\right)^T \lambda = \frac{dL}{d\tilde{u}}, \tag{25}$$

and the gradient is given by

$$\frac{dL}{d\xi} = -\left(\frac{\partial \tilde{R}}{\partial \xi}\right)^T \lambda \tag{26}$$

4.6 Basis library for twin model

Next, we consider choosing an appropriate basis library g. As mentioned in section 4.3, the basis functions can be chosen as a Volterra series. In this section we provide a different basis library from the viewpoint of multiresolution analysis. For simplicity, we start from a one dimensional function $F(\tilde{u})$, $\tilde{u} \in \mathbb{R}$. Theoretically, many fuction approximation methods can be chosen for g, such as polynomial approximation, Fourier series approximation, and wavelet approximation. We will focus on the wavelet approximation. In the following we will apply the theory of wavelet approximation to our problem, then we will discuss the reasons for choosing wavelet approximation.

Wavelet approximation can be explained by Mallat's *multiresolution analysis (MRA)* [26]. In one dimension, MRA is an increasing sequence of closed function spaces $\{V_j\}_{j\in\mathbb{Z}}$ which approximates $L^2(\mathbb{R})$. V_j approximates functions with increasing resolutions as j increases. The spaces satisfy the following properties:

$$\begin{aligned}
&\text{MRA 1} \quad && \cdots \subset V_{-1} \subset V_0 \subset V_1 \subset \cdots \\
&\text{MRA 2} \quad && \bigcup_{j\in\mathbb{Z}} V_j \text{ is dense in } L^2(\mathbb{R}) \\
&\text{MRA 3} \quad && f(x) \in V_j \Leftrightarrow f(2x) \in V_{j+1},\ j \in \mathbb{Z} \\
&\text{MRA 4} \quad && f(x) \in V_j \Leftrightarrow f(x - \frac{k}{2^j}) \in V_j,\ j \in \mathbb{Z},\ k \in \mathbb{Z}
\end{aligned}$$

In wavelet theory, the orthonormal basis for V_j is given by

$$\phi_{j,k}(x) = 2^{j/2}\phi(2^j x - k)\,, \quad k \in \mathbb{Z} \tag{27}$$

$\phi_{0,0}$ is called the *scaling function*. Projecting a function $f \in L^2(\mathbb{R})$ on the V_j gives

$$\begin{aligned}
P_{V_j} f &= \sum_{k\in\mathbb{Z}} \langle f, \phi_{j,k}\rangle\, \phi_{j,k} \\
&= \sum_{k\in\mathbb{Z}} \left(\int_{\mathbb{R}} f(x)\phi_{j,k}(x)\,\mathrm{d}x \right)\, \phi_{j,k}
\end{aligned} \tag{28}$$

Scaling functions can be either discontinuous (e.g. Haar wavelet [32]) or continuous (e.g. Meyer wavelet [33]). Because we desire differentiability of the twin model, we will focus on continuous scaling functions. As an example, we show the Meyer wavelet scaling function and its spectrum.

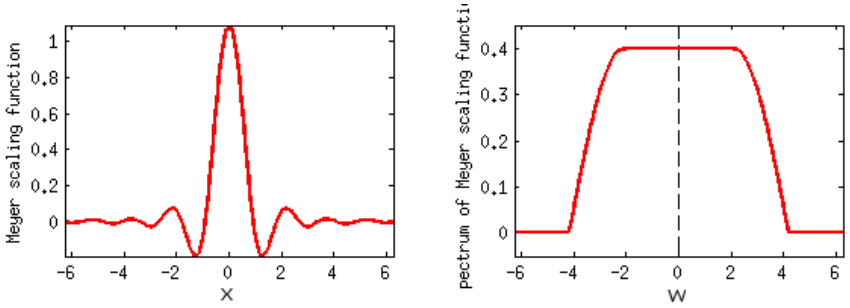

Figure 3: Meyer wavelet scaling function and its spectrum

$\phi_{j,k}(x)$ is localized in the frequency domain, and can be seen as a low pass filter. Projecting a function $f \in L^2(\mathbb{R})$ onto V_j gives a bandlimited approximation of f. As j increments by 1, the bandwidth of the low pass filter will increase by a factor of 2, so does the approximation resolution. Besides, $\phi_{j,k}(x)$ is localized in x, i.e. $\phi_{j,k}(x) \to 0$ as $x \to \pm\infty$. Given j and k, $\langle f, \phi_{j,k}\rangle$ effectively controls the shape of $P_{V_j} f$ only within a bounded domain centered at $\frac{k}{2^j}$. This will be an important property when we discuss the concept of *excited parameter domain* in section 4.8. In practice, it's infeasible and unnecessary to include all $\phi_{j,k}$ $k \in \mathbb{Z}$ into the basis library for a given j. For example, in the 1D water-oil displacement process [28], the water saturation u satisfies $0 \le u \le 1$. Therefore, it's unnecessary to consider k for which $\frac{k}{2^j} \gg 1$ or $\frac{k}{2^j} \ll 0$. We will discuss this topic in greater detail in section 4.8.

In Eqn(3) and Eqn(19), we notice that adding a constant to F's and g's does not change the equations. In other words, it suffices to approximate the flux functions' gradients instead of the flux function value. Therefore, we consider the following functions:

$$\bar{\phi}_{jk}(x) = \int_{-\infty}^{x} \phi_{j,k}(\tau)\,\mathrm{d}\tau \tag{29}$$

The gradient of $\bar{\phi}_{jk}(x)$ is local in frequency and local in x. In this section, we will use $\{\bar{\phi}_{jk}\}$, $k \in \mathbb{Z}$ with a fixed j as the basis library for the flux function.

For flux functions $F(\tilde{u})$, $\tilde{u} \in \mathbb{R}^n$, $n > 1$, the analogy of basis functions is straightforward. The MRA for $L^2(\mathbb{R}^n)$ is $V_{j_1} \otimes V_{j_2} \otimes \cdots \otimes V_{j_n}$, with $\{j_1, j_2, \cdots, j_n\} \in \mathbb{Z}^n$ [26, 66]. Given $\mathbf{j} = \{j_1, \cdots, j_n\}$, The basis is

$$\phi_{\mathbf{j},\mathbf{k}} = \phi_{j_1,k_1}(x_1) \cdots \phi_{j_n,k_n}(x_n), \quad \mathbf{k} \in \mathbb{Z}^n \tag{30}$$

Therefore, the basis for the twin model flux function is

$$\bar{\phi}_{\mathbf{j},\mathbf{k}} = \bar{\phi}_{j_1,k_1}(x_1) \cdots \bar{\phi}_{j_n,k_n}(x_n), \quad \mathbf{k} \in \mathbb{Z}^n \tag{31}$$

Below we plot $\bar{\phi}_{0,0}(x)$ and $\bar{\phi}_{\mathbf{0},\mathbf{0}}(x_1, x_2)$ integrated from Meyer scaling function.

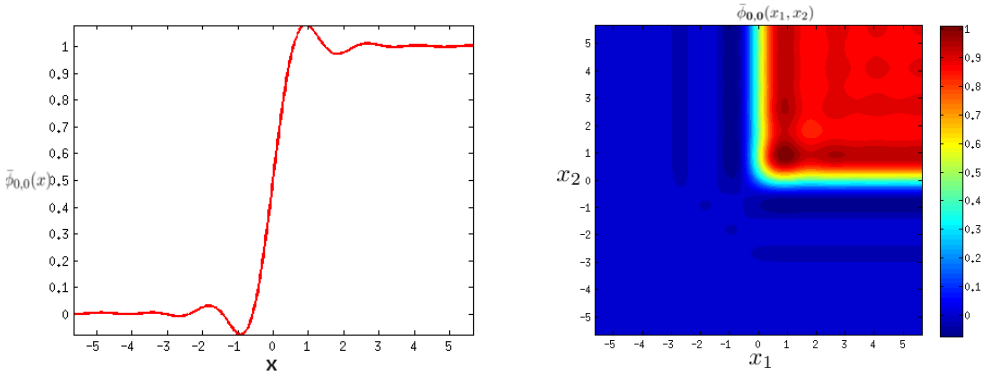

Figure 4: $\bar{\phi}_{0,0}$ in 1D and 2D, integrated from Meyer wavelet scaling function

Clearly, using Eqn(31) as the basis for the flux functions will be problematic for high dimensional $\mathbf{x}$. We will address this problem in section 4.8.

Although function approximation with wavelet scaling function has mathematical rigor, $\bar{\phi}$'s are not ideal bases for our problem. Firstly, the integral of 1D scaling function is rippled, as can be seen in the Meyer wavelet example. This is due to the *localization in frequency* property of scaling functions, known as the Gibbs phenomenon. The rippled flux may cause shock waves in hyperbolic equation simulations. Indeed, the property of localization in frequency is not necessary in our twin model problem. Secondly, generally $\bar{\phi}$ does not have an analytical expression. So $\bar{\phi}$ must be evaluated by numerical integration or interpolation using a lookup table, which can be more computationally intensive than anlytical expressions. Therefore, we prefer a *monotonic* and *analytical* approximation for $\bar{\phi}$.

We choose a sigmoid function to replace $\bar{\phi}_{0,0}$:

$$\bar{\phi}_{0,0}(x) = \frac{1}{2}\left(\tanh(\beta x) + 1\right), \tag{32}$$

where β is a constant determining the gradient of the function at $x = 0$. And

$$\bar{\phi}_{j,k}(x) = \frac{1}{2}\left\{\tanh\left(\beta(2^j x - k)\right) + 1\right\} \tag{33}$$

Or if we don't specify resolution on a dyadic grid 2^j, we can write Eqn(33) as

$$\bar{\phi}_{r,k}(x) = \frac{1}{2}\left\{\tanh\left(\beta(rx - k)\right) + 1\right\}, \tag{34}$$

where $r > 0$. Without further specifications we'll choose $\beta = 1.5$. Below we plot $\bar{\phi}_{0,0}(x)$ and $\bar{\phi}_{\mathbf{0},\mathbf{0}}(x_1, x_2)$ using the sigmoid function.

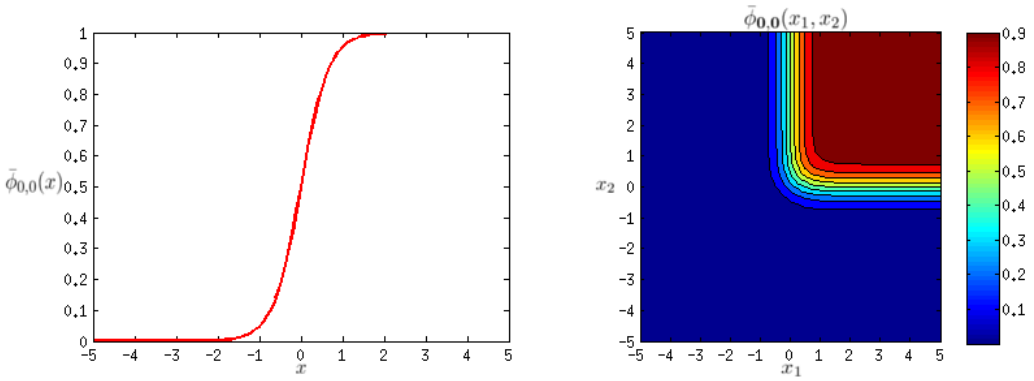

Figure 5: tanh *sigmoid function in 1D and 2D*

4.7 Numerical example: twin model with fixed structure

In this section we demonstrate a numerical example for fitting a twin model with fixed structure. Consider a 1D Buckley-Leverett equation

$$\frac{\partial u}{\partial t} + \frac{\partial F(u)}{\partial x} = 0 \quad x \in [0,1]\,,\ t \in [0,1] \tag{35}$$

with periodic boundary condition

$$u(x=0) = u(x=1) \tag{36}$$

and initial condition

$$u(t=0) = u_0 \tag{37}$$

Buckley-Leverett equation is a simple model for 1D, two-phase, porous media flow driven by capillary pressure and Darcy's law [28]. u indicates one phase's saturation and $0 \le u \le 1$. The flux function $F(u)$ depends on the phases and the porous media. A popular $F(u)$ is

$$F(u) = \frac{u^2}{1 + A(1-u)^2}\,, \tag{38}$$

where A is a constant. In the following we assume the blackbox simulation solves Eqn(35) with the flux given by Eqn(38), and $A = 2$.

Assume $F(u)$ is unknown, we will fit a twin model using the blackbox simulation. As discussed in section 4.4 and 4.6, the twin model can be written as

$$\frac{\partial \tilde{u}}{\partial t} + \frac{\partial}{\partial x}\left(\sum_{k=1}^{m} \xi_k \bar{\phi}_{r,k}(\tilde{u})\right) = 0 \tag{39}$$

with the same initial and boundary conditions. We will use Eqn(34) for $\bar{\phi}$. Both the black-box simulation and the twin model use a second order finite volume discretization and Crank-Nicolson time integration scheme.

We need to determine r and the range for k a prior. A larger r means higher resolution of the flux, but the twin model will be more computationally costly to fit. For this example, we specify $r = 10$. Besides, not all $k \in \mathbb{Z}$ are required in the twin model. As mentioned before, the gradient of each basis indexed by k is non-zero only around $[\frac{k}{r} - \frac{1}{\beta r}, \frac{k}{r} + \frac{1}{\beta r}]$. In our problem, $0 \le u \le 1$, so it suffices to choose corresponding k's. We will choose $k = -1, 0, \cdots, 11$.

The objective of fitting the twin model is given in Eqn(18), and is itself an optimization. We use an automatic differentiation module *numpad* [68] to compute $\frac{dJ}{d\xi_k}, k = 1, \cdots, m$. Since the gradient information is available, we consider using a quasi-Newton method for the optimization. Quasi-Newton

methods build the Hessian approximation iteratively using gradient, and can greatly accelerate convergence [71]. When the degree of freedom of the optimization is high, the memory required to store the Hessian matrix can be large. To reduce the memory requirement, we can use the *low-memory Broyden-Fletcher-Goldfarb-Shannon* (L-BFGS) algorithm [70, 73, 72]. L-BFGS approximates the Hessian using only the gradients at newer previous iterations, and inverse the approximated Hessian efficiently using the Sherman-Morrison formula. For this work, we use the implementation of L-BFGS in Nlopt [70].

Although the objective is to minimize $\sum_{i=1}^{N}\sum_{k=1}^{T}\left(\tilde{u}_{ik}-u_{ik}\right)^2\Delta t_k\left|\Delta\mathbf{x}_i\right|$, we will not use it as the objective function directly and perform optimization in one shot. If $\tilde{F}(u)$ deviates from $F(u)$ a lot, then $\tilde{u}(x,t)$ can deviate from $u(x,t)$ significantly even at a small t. Therefore, solving the twin model and its adjoint in $t=[0,T]$ without an educated $\tilde{F}(u)$ can be a waste of computation resources. To improve efficiency, we propose a progressive optimization procedure:

$\xi^*=\mathbf{0}$;
Set integers $2=i_1<\cdots<i_M=T$;
for $I=i_1,\cdots,i_M$ **do**
  Optimize

$$\xi^*\leftarrow\arg\min_{\xi}\sum_{i=1}^{N}\sum_{k=1}^{I}\left(\tilde{u}_{ik}-u_{ik}\right)^2\Delta t_k\left|\Delta\mathbf{x}_i\right|$$

  with initial guess ξ^*.
end

Algorithm 1: Progressive optimization procedure

Notice $k=1$ corresponds to the initial condition. Since the twin model uses the same initial condition as the black-box model, $\tilde{u}_{i1}-u_{i1}$ is always zero. Choosing the integer sequence $i_1,\cdots,i_M$ can be problem dependent. Our experience shows the sequence should be denser at small i, and sparser at larger i. The tolerance of each sub-optimization problem does not need to be tight, except for the last iteration where $I=T$. In our problem, we use $i_l=\min\left\{1+2^l,T\right\}$, a relative tolerance of 10%, and maximum 10 iterations for the sub-optimization problems.

The initial condition is shown in Fig 6. Notice u_0 does not cover the entire range of $0\le u\le 1$: we have $\max(u_0)=0.89$, $\min(u_0)=0.07$.

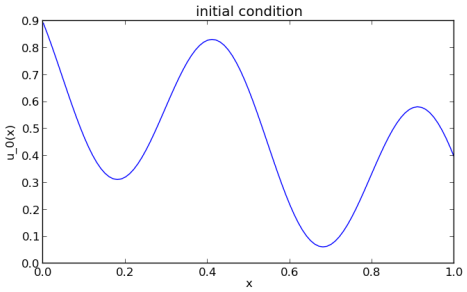

Figure 6: Initial condition $u_0(x)$

In Fig 7 we compare the converged twin model's flux $\tilde{F}(u)$ and its gradient $\frac{d\tilde{F}}{du}$ with $F(u)$ and $\frac{dF}{du}$. The range $u\in[\min(u(t,x)),\max(u(t,x))]$ is colored green.

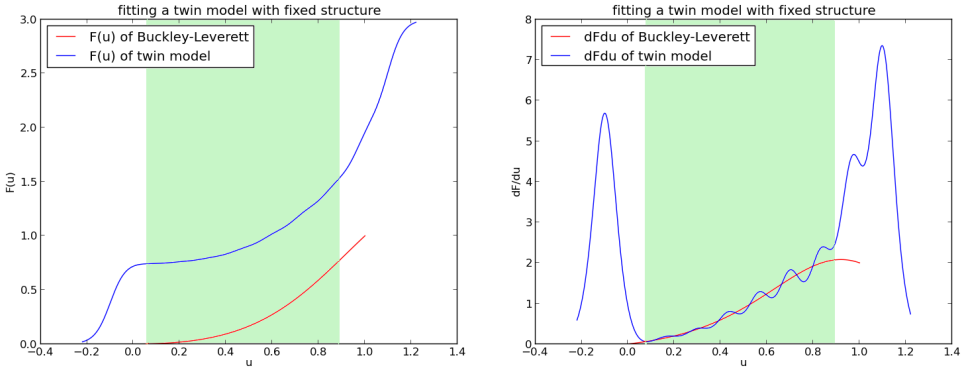

Figure 7: Compare $F(u)$ and $\frac{dF}{du}$ with $\tilde{F}(u)$ and $\frac{d\tilde{F}}{du}$

In Fig 8 we compare the solution $u(t,x)$ with the converged twin model's solution $\tilde{u}(t,x)$.

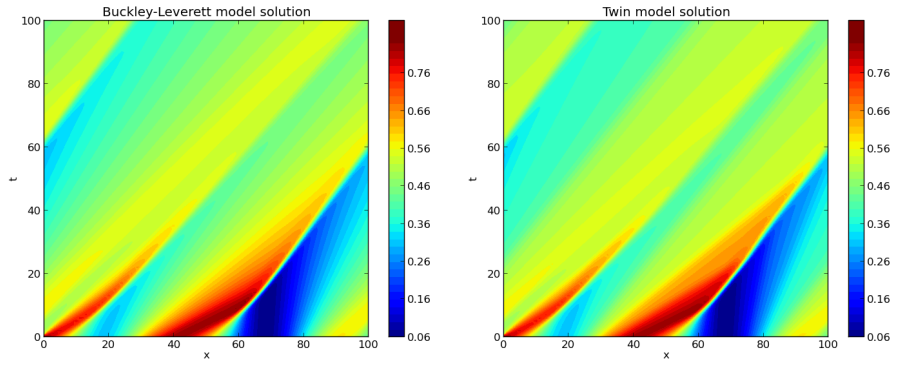

Figure 8: Compare $u(t,x)$ with $\tilde{u}(t,x)$

If we increase the flux resolution, the flux and the solution should have a better fit. For example, we use $r = 30$, $k = -3, \cdots, 33$. The flux comparison is shown in Fig 9

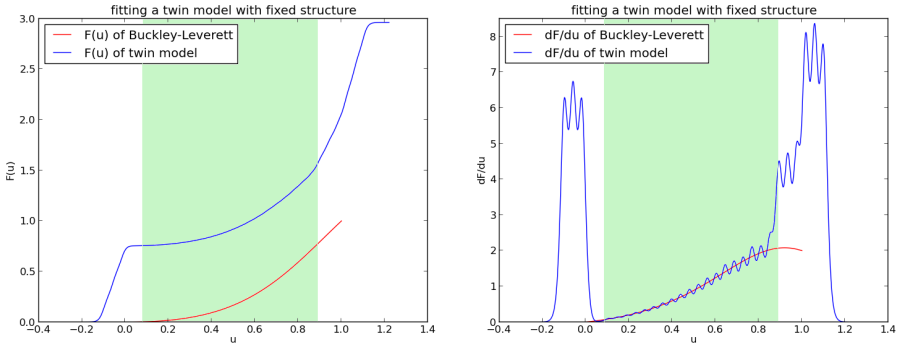

Figure 9: Compare $F(u)$ and $\frac{dF}{du}$ with $\tilde{F}(u)$ and $\frac{d\tilde{F}}{du}$ with higher flux resolution

The solution comparison is shown in Fig 10

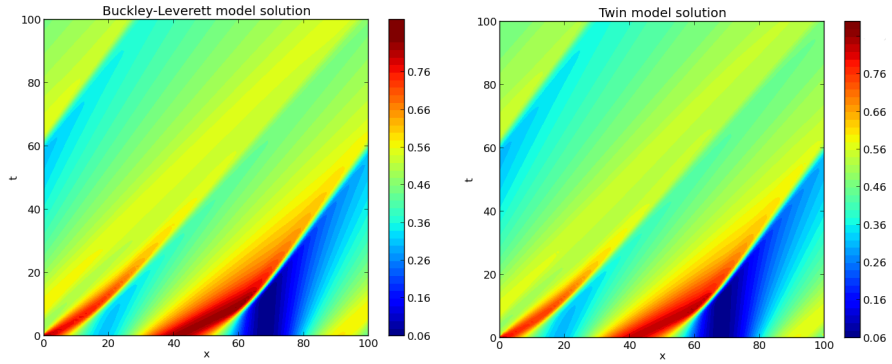

Figure 10: Compare $u(t,x)$ with $\tilde{u}(t,x)$ with higher flux resolution

Comparing Fig 7, 8 with Fig 9, 10, we observe a refined flux basis gives a more accurate twin model. However, we seek for an educated way to adaptively refine the basis and to control the computation cost. Therefore we will investigate *twin model with adaptive structure* in the next section.

4.8 Twin model with adaptive structure

A twin model with adaptive structure should be able to adaptively refine its basis $\bar{\phi}$ on-the-fly during fitting the basis coefficients ξ. For example, in section 4.7's numerical example, the value of $u(t,x)$, $t \in [0,T]$, $x \in [0,1]$ is bounded, i.e. $0 < u_{\min} \leq u(t,x) \leq u_{\max} < 1$; therefore as long as $\nabla\tilde{F}(u) = \nabla F(u)$ for $u \in [u_{min}, u_{max}]$, we will have $\tilde{u}(t,x) = u(t,x)$ for $t \in [0,T]$ and $x \in [0,1]$. In other words, in the numerical example, $\nabla\tilde{F}(u) = \nabla F(u)$ for $u \in [0,1]$ is a sufficient but not necessary condition for $\tilde{u}(t,x) = u(t,x)$. Intuitively, for some domains u, $\nabla\tilde{F}(u)$ has to approximate $\nabla F(u)$ accurately in order to give a good space-time solution match. We will call such domains *excited domain*, written as $\mathcal{E}$. Notice the excited domain is not a domain of space or time. Clearly $\mathcal{E}$ depends on $u(t,x)$. For u not inside $\mathcal{E}$, $\nabla\tilde{F}(u)$ will have little or no effect on the solution match; therefore we may not certify $\nabla\tilde{F}(u)$'s accuracy outside $\mathcal{E}$ no matter how closely the solutions match. As mentioned in section 4.6, we are interested in the problem of basis selection. Basis selections should only be navigated to $\mathcal{E}$.

To start with, consider a primal model solving the Eqn(3), and a twin model solving

$$\frac{\partial\tilde{u}(t,x)}{\partial t} + \nabla\cdot\tilde{F}(\mathcal{D}\tilde{u},\kappa) = q(\tilde{u},c(t,x))\,, \qquad i = 1,\cdots,n\,, \tag{40}$$

with the same initial condition, boundary condition, and controls. We define $\mathcal{E}$ by its complement $\bar{\mathcal{E}}$:

Definition 1. *Given a primal model, its discretized solution $u(t,x)$, and a twin model Eqn(40). The excited domain $\mathcal{E}$ is a domain of $\tilde{F}(\cdot)$. Let the complement of $\mathcal{E}$ be $\bar{\mathcal{E}}$. Consider a perturbed twin model flux $\tilde{F}_{\epsilon\delta}(\cdot) = F(\cdot) + \epsilon\delta(\cdot)$, $\epsilon \in \mathbb{R}, \delta \in L_2(\mathbb{R}^n)$. The perturbed twin model gives the discretized solution $\tilde{u}_{\epsilon\delta}$.*

A set $e \subseteq \bar{\mathcal{E}}$ if and only if

$$\frac{1}{T}\sum_{i=1}^{N}\sum_{k=1}^{T}\left(\tilde{u}_{\epsilon\delta,ik} - u_{ik}\right)^2 \Delta t_k \left|\Delta\mathbf{x}_i\right|$$

is independent of ϵ for any δ with support$[\delta] = e$.

This definition requires F a prior, therefore it is not directly implementable. In practice, we have to replace $\tilde{F}$'s baseline F with some approximation. The definition also requires enumeration of all possible δ to validate $\mathcal{E}$. In practice, we have to choose a finite set of δ, for example using the basis function library $\bar{\phi}$. However, even with a finite set of δ, we should not validate $\mathcal{E}$ with this definition numerically. As mentioned in section 4.7, unless $\tilde{u}(\tau)$ is reasonably close to $u(\tau)$, it does not make sense to keep

solving the twin model for $t > \tau$. Therefore, we should not let $\tilde{u}$ deviates from u a lot.

To restrict $\tilde{u}$ from large deviation to u, we propose a *global-local error* approach for basis selection. Define *global error*:

$$Err_G = \frac{1}{T}\sum_{i=1}^{N}\sum_{k=1}^{T}\left(\tilde{u}_{ik} - u_{ik}\right)^2 \Delta t_k \left|\Delta \mathbf{x}_i\right| \tag{41}$$

and *local error*:

$$Err_L = \frac{1}{T}\sum_{i=1}^{N}\sum_{k=1}^{T}\left(\tilde{u}'_{ik} - u_{ik}\right)^2 \Delta t_k \left|\Delta \mathbf{x}_i\right| \tag{42}$$

Here u is the *one-shot* solution of the twin model solving from $t = 0$ to $t = T$ with initial condition u_0. $\tilde{u}'_k$ is the solution of the twin model at $t = t_k$, solving from $t = t_{k-1}$ with initial condition u_{k-1}, for just one timestep. In other words, we solve $\tilde{u}'$ with restart for every timestep, whose initial condition is given by u at a previous timestep. We illustrate the idea in Fig 11.

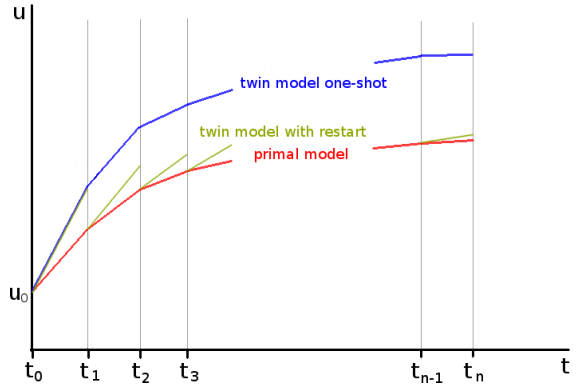

Figure 11: illustration of twin model with restart.

If we are able to bound Err_G with Err_L, we are guaranteed a good solution match even if we do not solve for the one-shot solution $\tilde{u}$. Under what condition can we bound Err_G? We give the following theorem.

Theorem 1. Consider the timestepwise mapping of the twin model

$$G : \mathbb{R}^n \mapsto \mathbb{R}^n,\ \tilde{u}^i \to G\tilde{u}^i = \tilde{u}^{i+1}\,, \quad i = 1, \cdots, n\,. \tag{43}$$

If G is a Lipschitz continuous mapping with constant α

$$\|Gx - Gy\|_{L_2} \leq \alpha \|x - y\|_{L_2} \tag{44}$$

then

$$Err_G \leq (1 + \alpha + \cdots + \alpha^{n-1}) Err_L\,. \tag{45}$$

If $\alpha < 1$, then

$$Err_G < \frac{1}{1-\alpha} Err_L \tag{46}$$

In practice, the assumption of $\alpha < 1$ may not be guaranteed. Therefore a small local error may not guarantee a small global error, for example for chaotic dynamical systems. Therefore, we only consider the local error as a tool to select basis, not a tool to finalize the twin model. After selecting the basis using the local error metric, we will still use the global error metric to fit the twin model, for example using algorithm 1.

Using the local error metric, we are able to reduce the twin model into solving a series of one-timestep problems with restart. But in each one-timestep problem, the numerical implementation of $\nabla\cdot$ in Eqn(40) is nonlinear. If we approximate $\nabla\cdot$ linearly, we will be able to use the wealth of knowledge of linear system basis selection. Let $\nabla\cdot$ be approximated by a finite difference operator D. Besides, a stable time integration scheme of twin model's solver is necessary for theorem 1 to hold. Here we let $\frac{\partial}{\partial t}$ be approximated by Backward Euler. Then Eqn(40) becomes

$$-\frac{1}{\Delta t_k}\left(\tilde{u}_k - \tilde{u}_{k-1}\right) + q(\tilde{u}_k, c(t_k)) = \sum_{i=1}^{m} \xi_i D\left(\bar{\phi}_i(\mathcal{D}\tilde{u}_k, \kappa)\right) , \quad k = 1, \cdots, T \tag{47}$$

For the kth timestep, let

$$P_{ki} = D\left(\bar{\phi}_i(\mathcal{D}\tilde{u}_k, \kappa)\right) \in \mathbb{R}^N , \tag{48}$$

where N is the number of spatial gridblocks, and i is the basis index. Also let

$$Y_k = -\frac{1}{\Delta t_k}\left(\tilde{u}_k - \tilde{u}_{k-1}\right) + q(\tilde{u}_k, c(t_k)) \in \mathbb{R}^N . \tag{49}$$

We rewrite Eqn(47) as

$$Y = P\xi , \tag{50}$$

where

$$P = \begin{pmatrix} P_{11} & \cdots & P_{1m} \\ \vdots & & \vdots \\ P_{T1} & \cdots & P_{Tm} \end{pmatrix}_{NT\times m} , \quad Y = \begin{pmatrix} Y_1 \\ \vdots \\ Y_T \end{pmatrix}_{NT} , \quad \xi = \begin{pmatrix} \xi_1 \\ \vdots \\ \xi_m \end{pmatrix}_{m} \tag{51}$$

Unlike linear regression, the objective of Eqn(50) is not to compute ξ, but to select a subset of variables of ξ. This is a *linear* variable dimensional reduction problem. Existing methods can be categorized into two classes [5]: One class is to rank the importance of the variables and to select a subset of important variables directly from candidate variables [79, 76]. Another class is to transform the original variables into a new reduced dimensional space [74]. One of the most popular methods of the second calss is principal component analysis (PCA) [77]. Although PCA can be efficiently computed by singular value decomposition, it has a disadvantage. Because the principal components depend on *all* original variables, they can be difficult to interpret [5]. In the twin model analysis, we want a basis selection scheme that reflects the excited domain $\mathcal{E}$. Therefore, we will focus on the first class of methods.

Linear variable selection is a rich field. It considers a linear model where each response variable y_i relates with predictors x_{ij} as follows

$$y_i = \xi_0 + \sum_{j=1^m} x_{ij}\xi_j + \epsilon_i , \quad i = 1, \cdots, N . \tag{52}$$

ϵ's are independent noises. Some of the m predictors may be unhelpful for predicting y, and can be deleted. The task of variable selection is to decide which subset of of variables should be deleted in order to get the *best* equation [80]

$$y_i = \xi_0 + \sum_{j\in\mathcal{S}\in 1,\cdots,m} x_{ij}\xi_j + \epsilon_i , \quad i = 1, \cdots, N . \tag{53}$$

Different metrics of defining 'best' lead to different variables selection recipes. We can by no means give a complete review of the methods here. Instead, we will only review two most popular classes of methods: *test-based methods*, and *regularization-based methods*.

Test-based methods implements a sequence of hypothesis tests to select variables. They include forward, backward, and stepwise sequential testings [81, 80]. Forward methods start with an empty set of selected variables, then sequentially add the most significant unselected variables, for example the forward orthogonal least squares method for variable selection [76]. Backward methods start with a full set of

selected variables, then prunes non-significant predictors one at a time. The stepwise methods alternate between adding and removing variables. However, there has been some critics to test-based methods [80]: Firstly, these methods select variables sequentially using a greedy approach. But the combinations of the best players at each step may not yield the best team. Secondly, the greedy heuristics do not have a firm justification in statistical theory. The testing-based methods attempt to find the best model without first defining what 'best' means.

In contrast, regularization-based methods first define a metric of model goodness, then search for the best model that maximize the metric. The metric is generally the *penalized log likelihood*:

$$\ell(\mathbf{x}, \mathbf{y}, \xi) - c(\xi)\,, \tag{54}$$

where ℓ is the likelihood, c is a measurement of model complexity. Generally the penalty term is

$$c(\xi) = \lambda \sum_{j=1}^{m} |\xi^q|^{1/q}\,, \quad \lambda > 0,\, 0 \leq q \leq 2 \tag{55}$$

It can be shown subset selection emerges as q is close to 0. Ridge regression chooses $q = 2$, and has no effect of variable selection. Methods based on Akaike information criterion (AIC) [83] and Bayesian information criterion (BIC) [84] chooses $q \to 0$, with different choices of λ. But they yields a non-convex problem which is less attractive for computation. Lasso chooses $q = 1$, which is the smallest value of q that yields a convex problem [79]. The properties of variable selection and computation efficiency motivate us to use Lasso to select basis.

We implement Lasso variable selection using a python module *sklearn* [69]. The result is shown in Fig 12 and Fig 13.

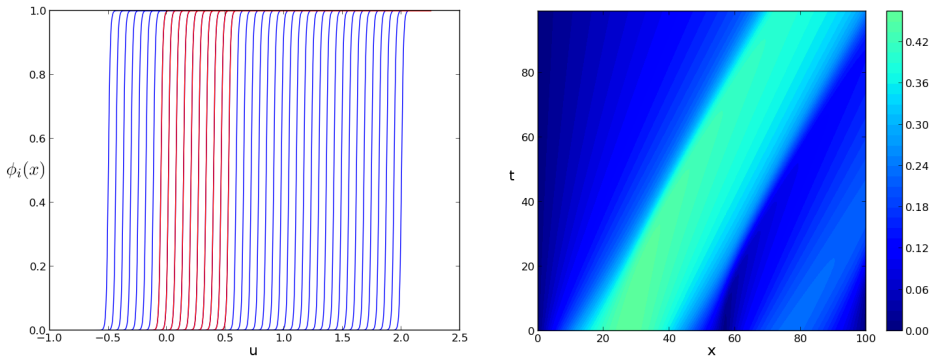

Figure 12: Basis selection using Lasso. The figure on the right side shows the primal model's solution $u(t, x)$. The figure on the left side shows all candidate bases. The selected bases are colored red. Notice how the selected bases correspond to the colorbar of the primal model solution.

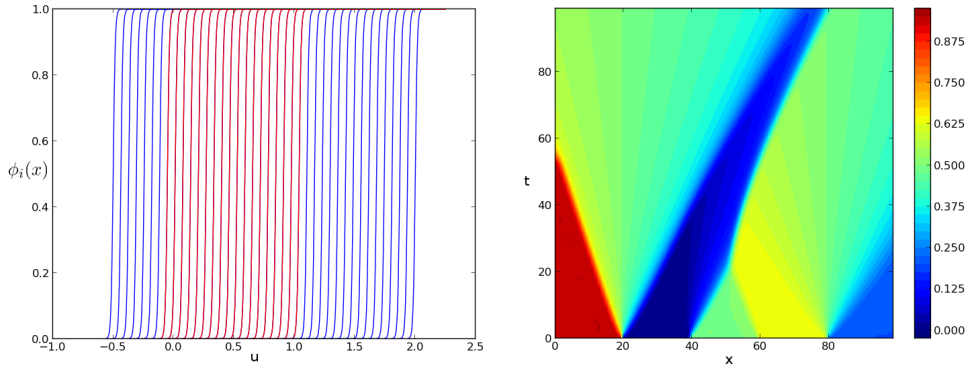

Figure 13: Basis selection with a different $u(t, x)$. Notice how selected bases depend on the primal model solution.

4.9 Future work

The sections above provide a framework to infer the twin model for time-dependent primal models with unknown flux functions. However, there are four issues to investigate.

Firstly, we need to extend the theory to more general problems. We should investigate twin models with unknown source term, and twin models with both unknown source term and flux function. Besides, we need to study time-independent (steady state) twin model. If we think of using time *dependent* twin model to match a video (time-space solution), then we use time *independent* twin model to match an image (space-only solution).

Secondly, we need to explore the weighting scheme used in Eqn(15). Loosely speaking, choosing $w = 1$ is equivalent to setting a uniform sample weight, where each 'sample' corresponds to the solution at a spatial and time grid point. By using a variable w, we should be able to fine tune the twin model accuracy at different locations in the excited domain $\mathcal{E}$. For example, should we assign a larger w for regions with sparser samples? Or should we assign a larger w for regions where more interesting physics happen (e.g. around a shock wave)? The weighting scheme may be ad hoc, but can possibly improve the twin model's accuracy for specific numerical examples.

Thirdly, in section 4.8, we discussed twin model with adaptive structure. The proposed approach constructs a *fixed* candidate basis library (Volterra series, wavelet scaling functions, and sigmoid functions), then selects a subset of basis from the library. However, the cardinality of the basis library can be high

for flux functions with a large number of inputs, for example $F(u_1, \cdots, u_n)$ with a large n. Besides, the proposed basis library may be inefficient to represent flux of the form $F(\mathbf{w}^T\mathbf{u})$, where $\mathbf{w}$ is a constant vector. Although $F(\mathbf{w}^T\mathbf{u})$ can be reduced to a univariate function by a change of variable $u^* = \mathbf{w}^T\mathbf{u} \in \mathbb{R}$, the fixed basis library can not take advantage of it. Therefore, the twin model method may be improved by choosing a set of basis from an *non-fixed* basis library. A literature survey is required to determine the most appropriate method to use.

Fourthly, we need to extend the basis selection scheme to time-independent PDEs. Right now, the basis selection scheme in section 4.8 is only for time-dependent PDEs. Using a global-local error approach and a finite difference approximation, the basis selection problem was reduced to a linear basis selection problem. If we want to infer a time-independent PDE, this approach is not applicable.

5 Optimization with twin model

In chapter 4, we developed twin model as a physics-based surrogate method. How should we leverage this surrogate to facilitate optimizations based on gray-box simulations? In this chapter, we answer this question by developing a provably convergent optimization scheme. We also demonstrate our method's superiority for optimization with high-dimensional controls.

5.1 Motivation of the Bayesian approach

We are interested in optimization problems of the following form

$$\begin{aligned} &\min_{c\in\mathcal{C}} J(u,c) \\ \text{where } u \text{ satisfies } &\ \mathcal{R}(u,c)=0 \\ \text{subject to } &\mathcal{C}=\left\{c\in\mathbb{R}^d \middle|\, Ac\le b, V(c)\le 0\right\} \end{aligned} \tag{56}$$

where $u(t,\mathbf{x})\in\mathbb{R}, t\in[0,T]$, $x\in\Omega$ is the space-time solution of a PDE abstracted as $\mathcal{R}$, with given initial and boundary conditions. The controls are $c\in\mathbb{R}^d$. There are l linear constraints defined by $A\in\mathbb{R}^{l\times d}$ and $b\in\mathbb{R}^l$ and s nonlinear constraints defined by $V(c)\in\mathbb{R}^s$. These linear and nonlinear constraints define a feasible region $\mathcal{C}\subseteq\mathbb{R}^d$. The evaluation of J for a given c requires solving the PDE $\mathcal{R}(u,c)=0$ which can be computational costly, such as large eddy simulation (LES) [93, 94] and direct numerical simulation (DNS) [95] in aerodynamic design problems. It is not uncommon for these simulations to take days, weeks, or even longer on a cluster. In addition to expensive evaluations of J, the evaluations of nonlinear constraints $V(c)$ can be similarly expensive. For example, in airfoil design we may aim at reducing drag while keeping lift above a threshold value [96]. Evaluating the lift of a given design requires simulating the flow. Besides, we consider the PDE and its solver as a gray-box. Finally, we consider controls of high dimension, i.e. $d\gg 1$.

We start with optimization problem Eqn(56) with feasible region $\mathcal{C}=\mathbb{R}^d$ for simplicity. There are already many methods that deal with such optimizations. But as mentioned in section 2.3, these methods are not suitable for our problem because they either require adjoint-based gradient of the PDE solver, or suffer from the curse of dimensionality. Can we utilize the twin model together with the primal model, and develop an optimization scheme that addresses these challenges?

The question fits naturally into a *multifidelity optimization (MFO)* framework. MFO performs optimization with multiple models ranging from low-fidelity to high-fidelity. Conventionally, low-fidelity models are cheaper to solve, but yield results with less credibility; high-fidelity models are more credible, but more expensive to solve. MFO balances computation investments between high- and low-fidelity models in order to reach optimum with overall less computation cost. In our problem, the primal model can be considered as a high-fidelity model, and the twin model can be considered as a low-fidelity model.

MFO methods can take various flavors. For example, an MFO method can be as simple as a two-stage optimization [86]. In the first stage it optimizes with the low-fidelity model only. In the second stage it optimizes with the high-fidelity model only, using the first stage optimum as the initial guess. However, we are only interested in *provably convergent* MFO methods. Based on our literature review, there are three types of such methods: *pattern search MFO*, *trust region MFO*, and *Bayesian MFO*. Each type can be viewed as extensions to their *single-fidelity* versions respectively, i.e. *pattern search methods*, *trust region methods*, and *Bayesian optimization methods*. In the following let's review these methods and their corresponding MFO methods.

In *pattern search methods*, the objective function J is evaluated at a set of trial points, called 'mesh', adjacent to the current best c in the design space. This step is called a 'poll step'. If improvement in J is obtained, the current best c is updated; otherwise, the mesh size is shrinked. These steps are iterated until convergence [89]. Pattern search methods can takes advantage of low-fidelity models to reduce computation cost, hereby *pattern search MFO*. It searches for improved design points using low-fidelity models before deciding whether to perform a poll step on the high-fidelity model [90]. However, each

poll step requires order d high-fidelity model evaluations, which can be too expensive to afford in our problem settings.

In *trust region methods*, a functional surrogate is firstly constructed from evaluations of J, then the surrogate is minimized within a trust-region to generate a candidate design point. Depending on the availability of $\frac{\partial J}{\partial c}$, the functional surrogate can either use the gradient information [11], or not use the gradient information [3, 13, 14]. When a low-fidelity model exists, the functional surrogate of J can be replaced by the low-fidelity model, hereby *trust region MFO* [38, 39]. To improve MFO performance and guarantee convergence, researchers have proposed using functional surrogates to account for the discrepancy $\Delta J = J_{high} - J_{low}$ between high- and low- fidelity models within the trust region [2, 91]. However, there are two problems with trust region MFO. Firstly, the convergence proof of such methods requires a condition called *fully-linearity* [13]. The fully-linearity condition bounds the deviation of $\frac{dJ}{dc}$ between the high- and low- fidelity models within the trust region. As mentioned in chapter 2, it can be hard to obtain the gradient from the primal model. Therefore, it can be hard to certify fully-linearity and to support the convergence proof. Secondly, at every iteration, only the model evaluations within or adjacent to a trust region is actually used [91]. In our problem settings, each high-fidelity model evaluation can be so expensive that we should use *all* high-fidelity evaluations available. Therefore, trust region MFO is not suitable for our problem settings too.

In *Bayesian optimization methods*, J as a function of c is assumed to be an unknown realization of a *Gaussian process*. Bayesian optimization starts from a prior distribution of J, and updates its posterior as new samples of $J(c)$ arrive. This procedure is also known as *Kriging* [10, 15]. Then it constructs an *acquisition function* $\rho : \mathcal{C} \mapsto \mathbb{R}\ ,\ c \to \rho(c)$ from the posterior, which measures the expected utility of investing the next sample at c. Finally, we choose the next sample as the maximizer of the acquisition function. Bayesian optimization iterates over the posterior-update step and the ρ-maximization step until convergence [85, 6]. There are two advantages of Bayesian optimization: Firstly, Bayesian optimization uses all available model evaluations to construct the posterior. Secondly, it balances *exploration* with *exploitation* elegantly. Given a set of samples $J(c)$, should we choose the next sample in a sparsely sampled region (exploration), or in a region adjacent to the current best sample (exploitation). Bayesian optimization makes a trade-off between exploration and exploitation via appropriate acquisition functions. This method is provably convergent to the global optimal under mild requirement of the objective function [27, 4].

When a low-fidelity model exists, Bayesian optimization methods can be extended to *Bayesian MFO*. Let the high-fidelity model's objective function be $J(c)$, and the low-fidelity model's objective function be $\tilde{J}(c)$. Bayesian MFO assumes both $J(c)$ and $\tilde{J}(c)$ are unknown realizations of (possibly different) Gaussian processes. Loosely speaking, by connecting the high- and low-fidelity models using a Bayesian framework, we can better predict the high-fidelity model using low-fidelity model evaluations. Bayesian MFO assumes a *Markov property* between $J(c)$ and $\tilde{J}(c)$ [8]:

$$p\left[J(c_0)\middle|\tilde{J}(c_0), \tilde{J}(c_1), \cdots, \tilde{J}(c_N)\right] = p\left[J(c_0)\middle|\tilde{J}(c_0)\right]\ , \quad N \in \mathbb{Z}^+\,, \tag{57}$$

where $p(\cdot|\cdot)$ indicates the posterior. In other words, if we want to predict J at c_0 using $\tilde{J}$, then it suffices to evaluate $\tilde{J}$ only at c_0; we will gain no further information on $J(c_0)$ by observing J at $c \neq c_0$. This assumption is intuitive, and proves to be very useful and convenient [7, 8]. By furthur assuming the Gaussian processes to be stationary, we can obtain

$$\tilde{J}(c) = \rho J(c) + \epsilon(c)\,, \tag{58}$$

where ρ is a constant and $\epsilon(\cdot)$ is a realization of a Gaussian process. Assume we have evaluated J at $\mathbf{c} = \{c_1, \cdots, c_{N_1}\}$, and $\tilde{J}$ at $\tilde{\mathbf{c}} = \{\tilde{c}_1, \cdots, \tilde{c}_{N_2}\}$, then the posterior of $J(c)$ can be constructed from the joint distribution

$$p\left(J(c), J(\mathbf{c}), \tilde{J}(\tilde{\mathbf{c}})\right) = \mathcal{N}\left(\begin{pmatrix} m \\ \mathbf{m} \\ \tilde{\mathbf{m}} \end{pmatrix},\ \begin{pmatrix} \mathrm{var}(J(c)) & \mathrm{cov}(J(c), J(\mathbf{c})) & \mathrm{cov}(J(c), \tilde{J}(\tilde{\mathbf{c}})) \\ \mathrm{cov}(J(\mathbf{c}), J(c)) & \mathrm{var}(J(\mathbf{c})) & \mathrm{cov}(J(\mathbf{c}), \tilde{J}(\tilde{\mathbf{c}})) \\ \mathrm{cov}(\tilde{J}(\tilde{\mathbf{c}}), J(c)) & \mathrm{cov}(J(\mathbf{c}), \tilde{J}(\tilde{\mathbf{c}})) & \mathrm{var}(\tilde{J}(\tilde{\mathbf{c}})) \end{pmatrix}\right) \tag{59}$$

where m is the mean of J, $\tilde{m}$ is the mean of $\tilde{J}$, $\mathbf{m} = m\mathbf{1}_{N_1}$, and $\tilde{\mathbf{m}} = \tilde{m}\mathbf{1}_{N_2}$. The variance-covariances, known as *kernels*, have to be selected *a* prior. However, these kernels are flexible in that they have tunable parameters known as *hyperparameters*, so realizations of the Gaussian processes can represent a wide class of functions [92]. The estimation of the hyperparameters and $\rho, m, \tilde{m}$ will be discussed below. The choice of kernels can be various, among the most popular ones are squared exponential kernel and Matern kernel [6]. Because of the additional information of $\tilde{J}(\tilde{\mathbf{c}})$, we can estimate $J(c)$ with less variance than using $J(\mathbf{c})$ alone. This procedure is also known as *coKriging* [16]. With the posterior obtained by the coKriging, Bayesian MFO maximizes the acquisition function to select the next design point c to evaluate J.

How should we apply our twin model to a Bayesian MFO framework? Naturally we would think of a coKriging approach using Eqn(59): We would first simulate the primal model as a high-fidelity model at an initial guess c_0. This gives us the space-time solution u_0 and the objective function $J(c_0)$. We can train the twin model with u_0 using methods proposed in chapter 4. The trained twin model, as a low-fidelity model, can be simulated to obtain $\tilde{J}$ at a set of new design points. Finally, the posterior of $J(c)$ can be constructed using the joint distribution Eqn(59). We may repeat these steps while re-training the twin model at updated design points.

However, this approach is not suitable for our problem settings. The twin model may not be very cheap to evaluate. Contrary to the conventional ideology: "low-fidelity model is cheap", the twin model can be expensive to simulate. Twin model is itself a PDE simulator. Unlike many commericial or open-source gray-box PDE simulators whose code is highly optimized for efficiency, the twin model code can be less efficient and more costly to solve. When the design space dimension d is high, explorations of the design space using evaluations of $\tilde{J}$ suffers from the curse of dimensionality too.

To unleash the power of twin model, we propose using the twin model's gradient $\frac{d\tilde{J}}{dc}$ instead of $\tilde{J}(c)$ for coKriging. The twin model is an open-box and has the adjoint capability to compute $\frac{d\tilde{J}}{dc}$. It has been shown that using the adjoint-based gradient information can reduce the number of function evaluations for Bayesian optimization [44, 40], especially when d is large. In our problem settings, we do not have access to the adjoint-based gradient $\frac{dJ}{dc}$, but it is possible to approximate $\frac{dJ}{dc}$ by $\frac{d\tilde{J}}{dc}$. We can't make general arguments about the approximation accuracy. Even if the twin model can reproduce the space-time solution of the primal model at a training design point, we can't ascertain that their adjoints are close, for example when the twin model solves a chaotic system. However, the theoretical flaw should not prohibit us from investigating practical applications of twin model. Besides, later we will show that our optimization scheme converges to the global optimal for the primal model, no matter how accurate or inaccurate the gradient approximation is.

Here is an example demonstrating why it can be promising to approximate $\frac{\partial J}{\partial u}$ with $\frac{\partial \tilde{J}}{\partial u}$. Consider the numerical example in section 4.7, where the primal model solves:

$$\frac{\partial \tilde{u}}{\partial t} + \frac{\partial}{\partial x}\left(F(u)\right) = c\,, \tag{60}$$

for $c = 0$, with $F(u)$ given by Eqn(38). We trained a twin model Eqn(39) using the space time solution. We are interest in the approximation quality of the twin model's gradient at c adjacent to $c = 0$. The result is shown in

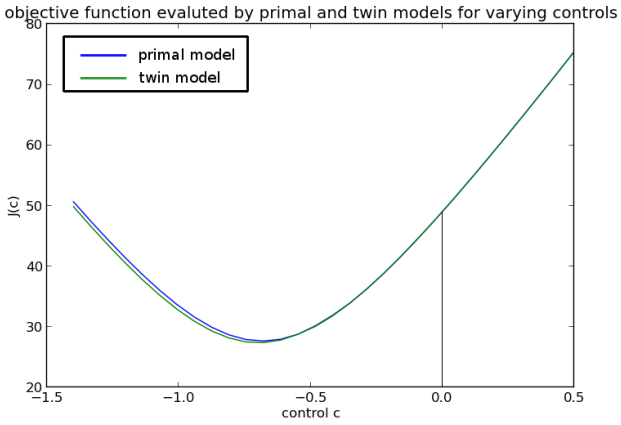

Figure 14: Train the twin model at $c = 0$, the resultant twin model gives good approximation for the $\frac{dJ}{dc}$.

The result is encouraging as the gradient computed by the twin model gives a good approximation of the gradient of the primal model. We reiterate that the good approximation quality benefits from the matching of space-time solution.

5.2 Bayesian modeling of the primal and twin models

We model the relation of $\nabla J(c)$ and $\nabla \tilde{J}(c)$ as

$$\nabla \tilde{J}(c) = \nabla J(c) + \epsilon(c)\,, \tag{61}$$

Assume $\nabla J(c)$, $\nabla \tilde{J}(c)$, and $\epsilon(c)$ are realizations of stationary Gaussian processes. We first model the priors of $\nabla J(c)$, $\nabla \tilde{J}(c)$, and $\epsilon(c)$, when no evalutions of the high- and low-fidelity models are made.

For any c_1 and c_2, assume $\epsilon(x)$ is an unknown realization of Gaussian process $\mathcal{N}(\mathbf{0}, K_\epsilon(\cdot,\cdot))$. $K_\epsilon : \mathbb{R}^n \times \mathbb{R}^n \mapsto \mathbb{R}$

$$K_\epsilon(c_1, c_2) = \boldsymbol{I}_{n\times n} k_\epsilon(c_1, c_2; \theta_\epsilon)\,, \tag{62}$$

where θ_ϵ are the hyperparameters of the kernel.
$J(c)$ is treated as a realization of the Gaussian process $\mathcal{N}(\mu, K(\cdot,\cdot))$, $K : \mathbb{R}^n \times \mathbb{R}^n \mapsto \mathbb{R}$ where

$$K(c_1, c_2) = k(c_1, c_2; \theta)\,. \tag{63}$$

θ are the hyperparameters of the kernel. Assume

$$\begin{aligned} cov(\nabla J(c_1), \epsilon(c_2)) &= 0 \\ cov(J(c_1), \epsilon(c_2)) &= 0\,, \end{aligned} \tag{64}$$

for any c_1, c_2. Then

$$cov(J(c_1), \nabla \tilde{J}(c_2)) = cov(J(c_1), \nabla J(c_2)) \tag{65}$$

for any c_1, c_2. There are multiple popular choices for the kernels. Generally the squared exponential kernel is a default choice. However, sample functions from this kernel are unrealistically smooth and may not represent the objective function well. Another popular choice is the Matern kernel, especially 5/2 kernel:

$$K_0(c_1, c_2; \theta) \equiv \sigma^2 \left(1 + \frac{\sqrt{5}d}{\rho} + \frac{5d^2}{3\rho^2}\right) \exp\left(-\frac{\sqrt{5}d}{\rho}\right)\,, \tag{66}$$

where $d = \|c_1 - c_2\|_{L_2}$. θ are the hyperparameters ρ and σ. The corresponding sample functions are twice differentiable, but not as smooth as the square exponential kernel. It has been shown the Matern

5/2 kernel outperforms other kernels in several Bayesian optimization problems [6]. Thus we choose the Matern 5/2 kernel as our choice. It is worth noting that the kernel function was chosen to be isotropic. In our problem, all the design parameters are the boundary points that controls the return bend geometry, so it makes sense to use a isotropic kernel for simplicity. In general, the metric d does not need to be isotropic, but this comes at the price of having more hyperparameters. Based on the assumptions above, we have

$$K_1(c_1, c_2; \theta) \equiv \frac{\partial}{\partial c_2} cov(J(c_1), J(c_2)) = \sigma^2 \exp\left\{-\frac{\sqrt{5}d}{\rho}\right\}\left(\frac{5}{3\rho^2} + \frac{5\sqrt{5}d}{3\rho^3}\right)(c_1 - c_2) \tag{67}$$

and

$$K_2(c_1, c_2; \theta) \equiv \frac{\partial^2}{\partial c_1 \partial c_2} cov(J(c_1), J(c_2)) = \sigma^2 \exp\left\{-\frac{\sqrt{5}d}{\rho}\right\}\left\{\left(\frac{5}{3\rho^2} + \frac{5\sqrt{5}d}{3\rho^3}\right)\boldsymbol{I} - \frac{25}{3\rho^4}(c_1 - c_2)(c_1 - c_2)^T\right\} \tag{68}$$

We will model $J(c)$ as sampled function with the kernel Eqn(66) with hyperparameters $\theta = (\rho, \sigma)$. We will model $\epsilon(c)$ as sampled function with the kernel

$$\boldsymbol{I}_{n\times n} K_0(c_1, c_2; \theta_\epsilon) \tag{69}$$

with hyperparameters $\theta_\epsilon = (\rho_\epsilon, \sigma_\epsilon)$. Suppose we sample J on $\mathbf{c}$, and sample $\nabla\tilde{J}$ on $\tilde{\mathbf{c}}$, then the joint probability of $J(c)$ at an unsampled c and the sampled data can be constructed. Specifically, the joint probability is a Guassian process with mean

$$(\mu, \boldsymbol{\mu}, \mathbf{0})^T \tag{70}$$

and covariance

$$\begin{pmatrix} K_0(c, c; \theta) & K_0(c, \mathbf{c}; \theta) & K_1(c, \tilde{\mathbf{c}}; \theta) \\ K_0(c, \mathbf{c}; \theta)^T & K_0(\mathbf{c}, \mathbf{c}; \theta) & K_1(\mathbf{c}, \tilde{\mathbf{c}}; \theta) \\ K_1(c, \tilde{\mathbf{c}}; \theta)^T & K_1(\mathbf{c}, \tilde{\mathbf{c}}; \theta)^T & K_2(\tilde{\mathbf{c}}, \tilde{\mathbf{c}}; \theta) + K_\epsilon(\tilde{\mathbf{c}}, \tilde{\mathbf{c}}; \theta_\epsilon) \end{pmatrix} \tag{71}$$

In practice, because the high-fidelity model is never simulated for infinite time to compute the time average, the sampling of J can be noisy. We assume the noise in sampling J due to finite high-fidelity simulation to be a white noise with variance δ_T^2, where T is the physical time running the high-fidelity simulation. Therefore, the covariance of the joint probability may be modified to

$$\begin{pmatrix} K_0(c, c; \theta) + \delta_T^2 & K_0(c, \mathbf{c}; \theta) & K_1(c, \tilde{\mathbf{c}}; \theta) \\ K_0(c, \mathbf{c}; \theta)^T & K_0(\mathbf{c}, \mathbf{c}; \theta) + \delta_T^2 \boldsymbol{I} & K_1(\mathbf{c}, \tilde{\mathbf{c}}; \theta) \\ K_1(c, \tilde{\mathbf{c}}; \theta)^T & K_1(\mathbf{c}, \tilde{\mathbf{c}}; \theta)^T & K_2(\tilde{\mathbf{c}}, \tilde{\mathbf{c}}; \theta) + K_\epsilon(\tilde{\mathbf{c}}, \tilde{\mathbf{c}}; \theta_\epsilon) \end{pmatrix} \tag{72}$$

The relationship of δ_T with T can be determined empirically.

5.3 Optimization using the posterior of the objective function

Using the assumptions in section 5.2, we can derive the posterior of $J(c)$ given samples of J and $\nabla\tilde{J}$. Then Bayesian optimization can be performed with the posterior. However, there are at least three questions to answer before applying Bayesian optimization. The first question is the choice of the acquisition function. The second question is how to optimize the acquisition function. The third question is how to determine the hyperparameters $\theta = (\sigma, \rho)$ and $\theta_\epsilon = (\sigma_\epsilon, \rho_\epsilon)$.

For the first question, generally people use two popular acquisition functions [6]. The first one is the *expected improvement* acquisition function. Let c_s^* be the best design after s previous samples $c_1, \cdots, c_s$, then the next sample c_{s+1} will be drawn with

$$c_{s+1} = \arg\max_{c\in\mathcal{C}} \mathbb{E}\left[\max\left(J(c) - J(c_s^*), 0\right) | \mathcal{S}\right], \tag{73}$$

where S indicates all available samplings on J and $\nabla\tilde{J}$. This formulation chooses the next sample point to maximize the expectation of the improvement: $\max\left(J(c) - J(c_s^*), 0\right)$ conditioned on existing samples,

hereby its name. Another popular method is the *upper confidence bound* acquisition function. The next sample is drawn with

$$c_{s+1} = \arg\max_{c\in\mathcal{C}} \left[\mu(J(c)\big|\mathcal{S}) + \kappa\sigma(J(c)\big|\mathcal{S})\right] , \tag{74}$$

with a tunable κ to balance exploration against exploitation. We will use the expected improvement formulation because it does not have the user tunable parameter κ. The formulation Eqn(73) has a close form under the Gaussian process assumption [6], which makes its evaluation straightforward.

For the second question, we consider using a gradient-driven optimizer with multiple initial guesses, for the following reasons. Firstly, the gradient of the acquisition function with respect to the candidate design point, $\frac{d\rho}{dc}$, can be obtained easily using automatic differentiation. Secondly, we want to reduce the risk of the optimization converging to a non-global-optimal candidate design, so it can be reasonable to optimize with multiple initial guesses. The specific optimizer is yet to be chosen, though we expect little impact on optimization performance due to different choices.

For the third question, there are two popular approaches to treat the hyperparameters. One approach is to use the maximum likelihood estimate of the hyperparameters, in which a point estimate of the hyperparameters are made by maximizing the likelihood function. Another approach is a Bayesian treatment of the hyperparameters. Instead of optimizing the acquisition function with a point estimate of the hyperparameters, it optimize an acquisition function marginalized over the hyperparameters, a.k.a integrated acquisition function. The marginalization is often implemented with an Monte Carlo approach [9]. Generally these two approach have comparible performance [6]. Without further specification our study is conducted using the maximum likelihood estimate approach.

To sum up, the proposed optimization flowchart is shown in Fig15

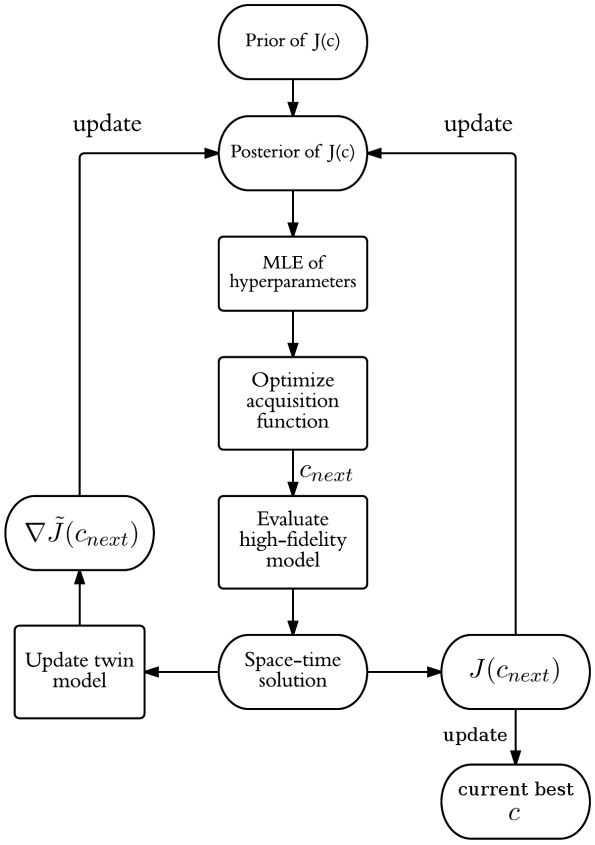

Figure 15: The flowchart of Bayesian optimization with twin model.

Intuitively, as the design space dimension increases, the ability to estimate $\frac{dJ}{dc}$ may become more important for faster J reduction. For illustration, we consider minimizing

$$J(x) = \sum_{i=1}^{\dim} x_i^2 \,. \tag{75}$$

The true optimal is $x = \mathbf{0}$. Suppose the evaluation of J is so expensive that we can only evaluate it for 10 times. When dim increases, we may expect the smallest J in the 10 evaluations to increase. When an estimation of $\frac{dJ}{dc}$ is available, the objective function may be reduced more quickly during the 10 evaluations, even if the gradient estimation is noisy. We demonstrate the superiority of using estimated gradient in Fig16.

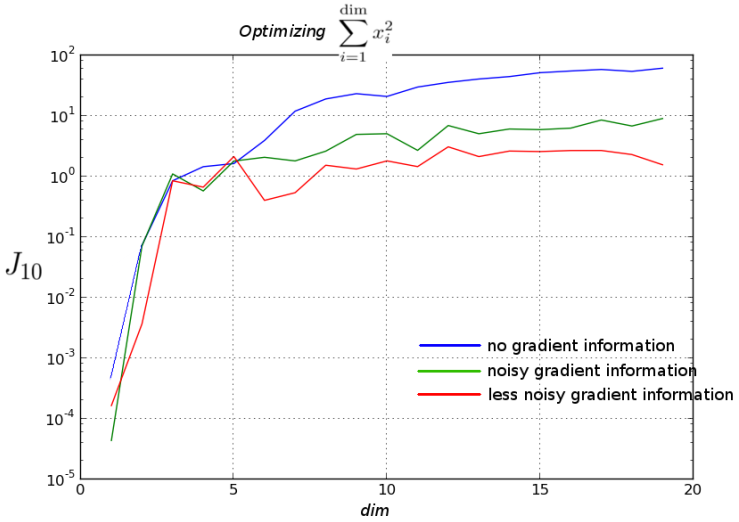

Figure 16: Minimizing $J(x) = \sum_{i=1}^{dim} x_i^2$ with variable dim. The y-axis is the best / smallest J after 10 function evaluations, in log 10 scale. The blue line is obtained from Bayesian optimization with no gradient information. The green line is obtained from Bayesian optimization with a noisy gradient, by setting $\sigma^2 = \sigma_\epsilon^2$, see Eqn(66) and Eqn(69). The red line is obtained from Bayesian optimization with a less noisy gradient, by setting $0.1\sigma^2 = \sigma_\epsilon^2$ We use Monte Carlo to randomly select some initial guesses for x. Each point on these lines represents the averaged J_{10} using a random set of initial guesses.

5.4 Discussion of the convergence property

Bayesian optimization is a deterministic global optimization strategy. Given previous evaluations, it locates deterministically the next design point for evaluation. In the end, the optimization generates an infinite sequence of design points. Clearly, given an optimization strategy, the sequence depends on the underlying function to evaluate, and depends on the initial design. The convergence property of Bayesian optimization can be discussed by the property of the design sequence, using the following theorem [99]:

Theorem 2. Let $W^{k,p}(\mathcal{X})$ be a Sobolev space of functions defined on $\mathcal{X}$. For any initial design in $\mathcal{X}$, a global optimization algorithm converges for all functions in $W^{k,p}(\mathcal{X})$ if and only if the design sequence produced by the algorithm is dense in $\mathcal{X}$ for all functions in $W^{k,p}(\mathcal{X})$.

Therefore, we will investigate whether the sequence produced by the proposed optimization scheme is dense. If we can sample the exact function value, and if we use the expected improvement acquisition function, it has been shown [4, 27] the sequence is indeed dense, under some mild conditions on the objective function. In this section, we extend the theoretical result to sample both the exact function value and the noisy function gradient.

Theorem 3. Assume

1. $\mathcal{X} \in \mathbb{R}^n$, $\|\cdot\|$ be the L_2 norm defined on $\mathcal{X}$.
2. $\mathcal{H}$ and $\mathcal{H}'$ be two reproducing kernel Hilbert spaces on $\mathcal{X}$, with kernels $K(\cdot,\cdot) : \mathcal{X} \times \mathcal{X} \mapsto \mathbb{R}$ and $K'(\cdot,\cdot) : \mathcal{X} \times \mathcal{X} \mapsto \mathbb{R}^n$ respectively.
3. There exist $k : \mathbb{R}^+ \bigcup \{0\} \mapsto \mathbb{R}$ and $k' : \mathbb{R}^+ \bigcup \{0\} \mapsto \mathbb{R}^n$, such that K and K' satisfies $K(x,y) = k(\|x-y\|)$ and $K'(x,y) = k'(\|x-y\|)$ respectively, for $\forall x, y \in \mathcal{X}$.
4. k and k' has the Fourier transforms $\hat{k}$ and $\hat{k}'$ respectively. Let $\hat{k}' = \left(\hat{k}'_1, \cdots, \hat{k}'_n\right)^T$. They satisfy the asymptotic properties $\hat{k}(u) = \Theta(|u|^{-n-2\nu})$ and $\hat{k}'_i(u) = \Theta(|u|^{-n-2\nu'})$, $i = 1, \cdots, n$ as $|u| \to \infty$, with $\frac{1}{2} < \nu < \infty$ and $\nu' = \nu - 1$. (Θ is the asymptotic big Θ notation.)

Let

1. $f \in \mathcal{H}$ be the underlying objective function to maximize.
2. $g \in \mathcal{H}'$ be the noisy gradient of f.
3. ϵ be the gradient sample noise
$$\epsilon = g - \nabla f \,.$$

Let the optimization strategy generates the design sequence according to

$$\begin{aligned} x_{s+1} &= \arg\max_{x \in \mathcal{X}} \mathbb{E}\left[\max\left(f(x) - f(x_s^*)\right) \middle| \mathcal{S}\right] \\ x_s^* &= \arg\max_{x \in \{x_1, \cdots, x_s\}} f(x) \\ \mathcal{S} &= \left\{ \{x_1, \cdots, x_s\}, \{f(x_1), \cdots, f(x_s)\}, \{g(x_1), \cdots, g(x_s)\} \right\} \end{aligned}$$

Then the sequence $\{x_1, x_2, \cdots\}$ is dense in $\mathcal{X}$ for $\forall x_1 \in \mathcal{X}$.

As a future work, we will prove the theorem in appendix B.

5.5 Optimization constraints

In the previous sections, we considered only non-constraint optimization for simplicity. In order to deal with the more general formulation Eqn(56), we need to consider inequality constraint optimization. Inequality constraint optimization is of great interest in the engineering community. For example, in the design of internal cooling ducts in turbomachineries, one possible objective is to minimize the pressure loss in a 180-degree return bend. However, reducing pressure loss may also reduce heat transfer, thus reduce the cooling ability [97, 98]. Therefore, a viable approach is to set a minimum heat transfer constraint while minimizing pressure loss. Another possible constraint in the internal cooling duct problem is the geometric bound on the duct's wall. This is because the duct must be contained inside the airfoil, and must be geometrically compatible with other components. We illustrate such a constraint in Fig 17.

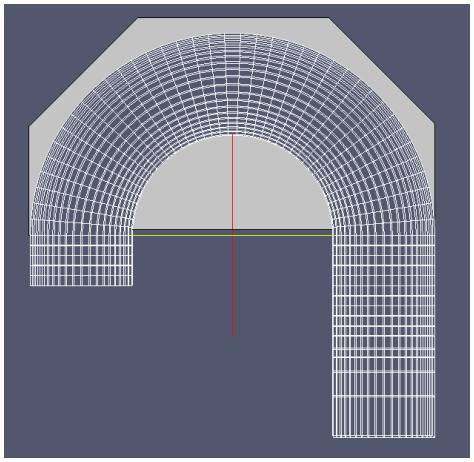

Figure 17: Example of a constraint of the feasible geometry, The brighter region indicates feasible region of the return bend geometry. The wireframe indicates a feasible design.

Constraints can be categorized into two types based on how they are evaluated: the first type are constraints that require a PDE simulations's space-time solution; the second type are constraints that do *not* require the space-time solution. In the example above, the constraint on the heat transfer belongs to the first type, while the constraint on the duct geometry belongs to the second type. Generally, evaluation of the first type constraint is much more expensive than the second type constraint, and can be similarly expensive as the evaluation of the objective function. Let the feasible region specified by the first type constraints be $\mathcal{C}_1$, and let the feasible region specified by the second type constraints be $\mathcal{C}_2$. The feasible region in Eqn(56) is $\mathcal{C} = \mathcal{C}_1 \bigcap \mathcal{C}_2$.

The second type constraints are not the topic of my research, because generally they can be evaluated cheaply. Optimization modules such as NLopt[70] have already implemented many established methods for such constraints. In Bayesian optimization, this type of constraints can be implemented in the optimization of the acquisition function, so the next evaluation point is always inside $\mathcal{C}_2$. The first type constraints, however, require special attention. If we choose the expected improvement formulation in our Bayesian optimization, Eqn(73) should be modified to:

$$c_{s+1} = \arg\max_{c \in \mathcal{C}_2} \left\{ \mathbb{E}\left[\max\left(J(c) - J(c_s^*), 0\right) \Big| \mathcal{S} \right] \cdot \mathbb{P}\big[V(c) \leq 0 \big| \mathcal{S}\big] \right\}, \tag{76}$$

The modified formulation is called *constraint expected improvement* [78]. Here c_s^* is the best *feasible* design in the previous s iterations. Notice the optimization domain is $c \in \mathcal{C}_2$. Intuitively, improvement on J is not counted valid unless the design is feasible.

Similar to $J(c)$, we can construct a posterior distribution on $V(c)$ and evaluate $\mathbb{P}\big[V(c) \leq 0 \big| \mathcal{S}\big]$ in Eqn(76). Straightforward evaluations of $V(c)$ using the primal model can be costly. However, similar to $J(c)$, we can use the twin model to estimate the gradient of $V(c)$ cheaply. Specifically, we construct the posterior of $V(c)$ using evaluations of $V(c)$ and $\frac{d\tilde{V}(c)}{dc}$, and use Eqn(76) as our acquisition function to perform optimization. The framework is shown in Fig 18.

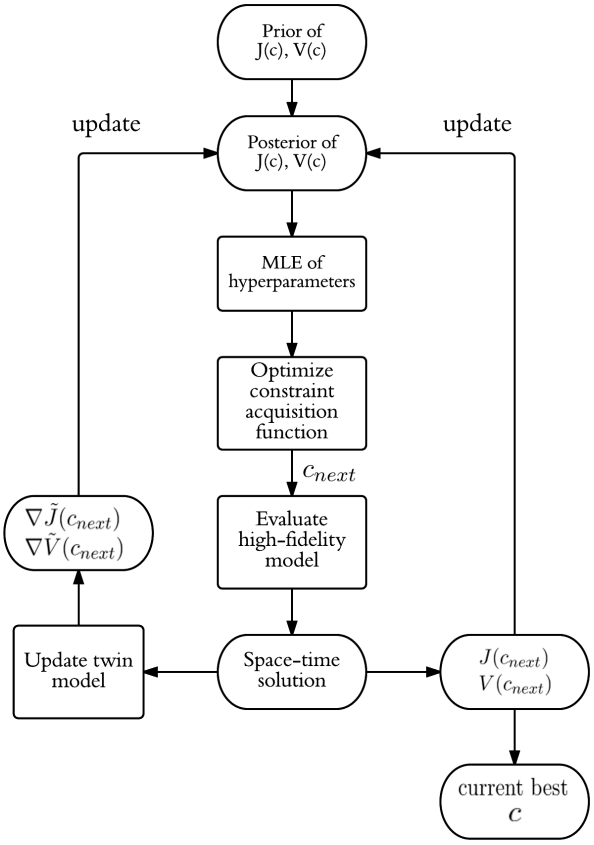

Figure 18: The flowchart of constraint Bayesian optimization with twin model.

5.6 Application to a return bend

High-fidelity turbulence simulation and RANS twin model
Fit for a twin model for the Reynold stress in RANS model. Consider twin model as a one-equation model.

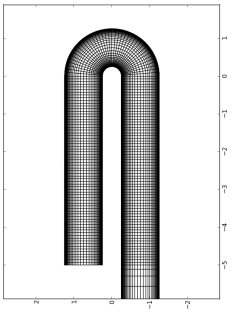

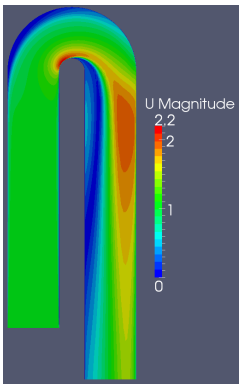

Appendices

A Proof of theorem 1: global-local error

Proof: Consider a primal model and a twin model solving for the space-time solution u and $\tilde{u}$ on the same time grid $\{t_0 = 0, t_1, \cdots, t_n = T\}$. The solutions at timestep t_i are u_i and $\tilde{u}_i$. Both simulations starts from the same initial condition u_0. Define the mapping of the primal model

$$H : \mathbb{R}^n \mapsto \mathbb{R}^n,\ u^i \to Hu^i = u^{i+1}\,, \quad i = 1, \cdots, n \tag{77}$$

and the mapping of the twin model

$$G : \mathbb{R}^n \mapsto \mathbb{R}^n,\ \tilde{u}^i \to G\tilde{u}^i = \tilde{u}^{i+1}\,, \quad i = 1, \cdots, n \tag{78}$$

G and H are linear or nonlinear mappings. We illustrate these mappings in Fig 19.

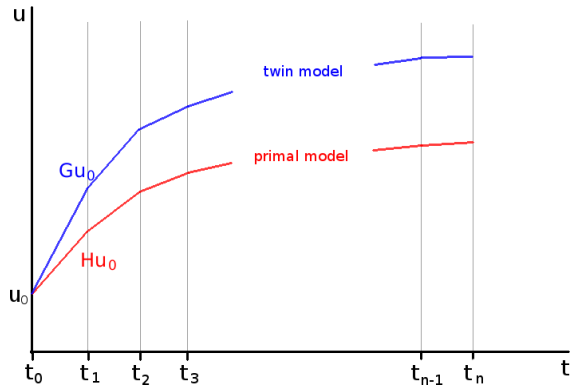

Figure 19: Trajectories of the primal model and the twin model. H and G are their timestep-wise mapping functions.

The global error is

$$Err_G = \frac{1}{n\Delta t}\left\{\|(G^n - H^n)u_0\| + \|(G^{n-1} - H^{n-1})u_0\| + \cdots + \|(G^1 - H^1)u_0\|\right\} \tag{79}$$

The local error is

$$Err_L = \frac{1}{n\Delta t}\left\{\|\left(GH^{n-1} - H^n\right)u_0\| + \|\left(GH^{n-2} - H^{n-1}\right)u_0\| + \cdots + \|\left(G^1 - H^1\right)u_0\|\right\} \tag{80}$$

Using the equality

$$G^i - H^i = (G^i - G^{i-1}H) + (G^{i-1}H - G^{i-2}H^2) + \cdots + (GH^{i-1} - H^i)\,, \quad i \in \mathbb{Z}^+\,, \tag{81}$$

we derive from Eqn(79)

$$Err_G \le \frac{1}{n\Delta t}\left\{\begin{array}{lll} \|(G^{n-1}G - G^{n-1}H)u_0\| + \|(G^{n-2}GH - G^{n-2}H^2)u_0\| & +\cdots+ \|(GH^{n-1} - H^n)u_0\| \\ + \|(G^{n-2}G - G^{n-2}H)u_0\| & +\cdots+ \|(GH^{n-2} - H^{n-1})u_0\| \\ \ddots & \vdots \\ & + \|(G - H)u_0\| \end{array}\right\} \tag{82}$$

Using Eqn(82) and Eqn(80), we get

$$Err_G - Err_L \leq \frac{1}{n\Delta t} \left\{ \begin{array}{lll} \|(G^{n-1}G - G^{n-1}H)u_0\| + \|(G^{n-2}GH - G^{n-2}H^2)u_0\| & + \cdots + \|(GGH^{n-2} - GH^{n-1})u_0\| \\ + \|(G^{n-2}G - G^{n-2}H)u_0\| & + \cdots + \|(GGH^{n-3} - GH^{n-2})u_0\| \\ \ddots & \vdots \\ & + \|(GG - GH)u_0\| \end{array} \right\} \tag{83}$$

Apply our assumption

$$\|Gx - Gy\| \leq \alpha \|x - y\| \tag{84}$$

and its implication

$$\left\|G^i x - G^i y\right\| \leq \alpha^i \|x - y\|, \quad i \in \mathbb{Z}^+ \tag{85}$$

to Eqn(86), we get

$$Err_G - Err_L \leq \frac{1}{n\Delta t} \left\{ \begin{array}{lll} \alpha^{n-1}\|(G - H)u_0\| + \alpha^{n-2}\|(GH - H^2)u_0\| & + \cdots + \alpha\|(GH^{n-2} - H^{n-1})u_0\| \\ + \alpha^{n-2}\|(G - H)u_0\| & + \cdots + \alpha\|(GH^{n-3} - H^{n-2})u_0\| \\ \ddots & \vdots \\ & + \alpha\|(G - H)u_0\| \end{array} \right\} \tag{86}$$

Reorder the summation, we get

$$Err_G - Err_L \leq \frac{1}{n\Delta t} \left\{ \begin{array}{lll} \alpha^{n-1}\|(G - H)u_0\| + \alpha^{n-2}\|(G - H)u_0\| & + \cdots + \alpha\|(G - H)u_0\| \\ + \alpha^{n-2}\|(GH - H^2)u_0\| & + \cdots + \alpha\|(GH - H^2)u_0\| \\ \ddots & \vdots \\ & + \alpha\|(GH^{n-2} - H^{n-1})u_0\| \end{array} \right\} \tag{87}$$

Therefore, from Eqn(87) and Eqn(80), we get

$$Err_G \leq (1 + \alpha + \cdots + \alpha^{n-1}) Err_L \,. \tag{88}$$

If $|\alpha|$ is strictly less than 1,

$$Err_G \leq \frac{1}{1 - \alpha} Err_L \,, \tag{89}$$

which completes the proof. □

B Proof of theorem 3: optimization convergence

To be proven.

References

[1] Han Chen. "Blackbox stencil interpolation method for model reduction" Master thesis, 2012

[2] March, Andrew, Karen Willcox, and Qiqi Wang. "Gradient-based multifidelity optimisation for aircraft design using Bayesian model calibration." Aeronautical Journal 115.1174 (2011): 729.

[3] Jones, Donald R., Matthias Schonlau, and William J. Welch. "Efficient global optimization of expensive black-box functions." Journal of Global optimization 13.4 (1998): 455-492.

[4] Bull, Adam D. "Convergence rates of efficient global optimization algorithms." The Journal of Machine Learning Research 12 (2011): 2879-2904.

[5] Stephen A Billings. "Nonlinear System Identification, NARMAX methods in time, frequency and spatial-temporal domains" ISBN:978-1-119-94359-4, 2013

[6] Snoek, Jasper, Hugo Larochelle, and Ryan P. Adams. "Practical Bayesian optimization of machine learning algorithms." Advances in Neural Information Processing Systems. 2012.

[7] Kennedy, Marc C., and Anthony O'Hagan. "Predicting the output from a complex computer code when fast approximations are available." Biometrika 87.1 (2000): 1-13.

[8] A. O'Hagan "A Markov property for covariance structures." Nottingham University Statistics Research Report 13 (1998).

[9] Murray, Iain, and Ryan P. Adams. "Slice sampling covariance hyperparameters of latent Gaussian models." Advances in Neural Information Processing Systems. 2010.

[10] Oliver, Margaret A., and R. Webster. "Kriging: a method of interpolation for geographical information systems." International Journal of Geographical Information System 4.3 (1990): 313-332.

[11] Carter, Richard G. "Numerical experience with a class of algorithms for nonlinear optimization using inexact function and gradient information." SIAM Journal on Scientific Computing 14.2 (1993): 368-388.

[12] Dembo, Ron S., Stanley C. Eisenstat, and Trond Steihaug. "Inexact newton methods." SIAM Journal on Numerical analysis 19.2 (1982): 400-408.

[13] Conn, Andrew R., Katya Scheinberg, and Lus N. Vicente. "Global convergence of general derivative-free trust-region algorithms to first-and second-order critical points." SIAM Journal on Optimization 20.1 (2009): 387-415.

[14] Wild, Stefan M., and Christine Shoemaker. "Global convergence of radial basis function trust-region algorithms for derivative-free optimization." SIAM Review 55.2 (2013): 349-371.

[15] G.M. Matheron, "Principles of geostatistics". Economic Geology 58.8 (1963): 1246-1266

[16] Goovaerts, Pierre. "Ordinary cokriging revisited." Mathematical Geology 30.1 (1998): 21-42.

[17] Christopher M. Bishop Pattern recognition and machine learning ISBN: 978-0387310732. 2007

[18] Sarma, Pallav, LJ Durlofsky, K Aziz, WH Chen. "Efficient real-time reservoir management using adjoint-based optimal control and model updating." Computational Geosciences 10.1 (2006): 3-36.

[19] Rios, Luis Miguel, and Nikolaos V. Sahinidis. "Derivative-free optimization: A review of algorithms and comparison of software implementations." Journal of Global Optimization 56.3 (2013): 1247-1293.

[20] Powell, Warren B. "Approximate Dynamic Programming: Solving the curses of dimensionality". Vol. 703. John Wiley & Sons, 2007.

[21] Dennis, Jr, John E., and Jorge J. Mor. "Quasi-Newton methods, motivation and theory." SIAM review 19.1 (1977): 46-89.

[22] Plessix, R-E. "A review of the adjoint-state method for computing the gradient of a functional with geophysical applications." Geophysical Journal International 167.2 (2006): 495-503.

[23] Nadarajah, Siva, and Antony Jameson. "A comparison of the continuous and discrete adjoint approach to automatic aerodynamic optimization." AIAA paper 667 (2000): 2000.

[24] A Griewank, GF Corliss Automatic differentiation of algorithms: theory, implementation, and application. Defense Technical Information Center, 1992.

[25] Zhangxin Chen "Reservoir Simulation: Mathematical Techniques in Oil Recovery" Society for Industrial and Applied Mathematics, ISBN 0898716403, 2007

[26] Mallat, Stephane G. "A theory for multiresolution signal decomposition: the wavelet representation." Pattern Analysis and Machine Intelligence, IEEE Transactions on 11.7 (1989): 674-693.

[27] Vazquez, Emmanuel, and Julien Bect. "Convergence properties of the expected improvement algorithm with fixed mean and covariance functions." Journal of Statistical Planning and inference 140.11 (2010): 3088-3095.

[28] S.E. Buckley and M.C. Leverett "Mechanism of fluid displacement in sands." Transactions of the AIME 146 (1942): 107-116

[29] Chen, Zhangxin, Guanren Huan, and Yuanle Ma. "Computational methods for multiphase flows in porous media." Vol. 2. Siam, 2006.

[30] Stephen Boyd and Lieven Vandenberghe "Convex Optimization" Cambridge University Press, 2004

[31] G. Cybenko "Approximation by superpositions of a sigmoid function" Mathematics of control, signals and systems 2.4 (1989): 303-314

[32] Alfred Haar "On the theory of orthogonal function systems" Mathematische Annalen 69 (1910): 331-371

[33] V.VV. Vermehren, H.M. de Oliveira "Close expressions for Meyer wavelet and scale function" arXiv:1502.00161 [stat.ME]

[34] Slawomir Koziel, Xin-She Yang "Computational optimization, methods and algorithms" Springer Berlin Heidelberg, 2011

[35] N.V. Queipo, R.T. Haftka, W. Shyy, T. Goel, R. Vaidynathan, P.K Tucker "Surrogate-based analysis and optimization" Progress in Aerospace Sciences 41 (2005): 1-28

[36] T.D. Robinson, M.S. Eldred, K.E. Willcox, R. Haimes "Surrogate-based optimization using multifidelity models with variable parameterization and corrected space mapping" AIAA Journal 46 (2008): 2814-2822

[37] Mohamed H. Bakr, John W. Bandler "An introduction to the space mapping technique" Optimization and Engineering 2 (2011): 369-384

[38] N.M. Alexandrov, E.J. Nielsen, R.M. Lewis, W.K. Anderson "First-Order Model Management with Variable-Fidelity Physics Applied to Multi-Element Airfoil Optimization" 8th AIAA Symposium on Multidisciplinary Design and Optimization (2000)

[39] N.M. Alexandrov, R.M. Lewis, C.R. Gumbert, L.L. Green, P.A. Newmann "Optimization with Variable-Fidelity Models Applied to Wing Design" 38th Aerospace Sciences Meeting (2000)

[40] Han Zhong-Hua, Stefan Grtz, Ralf Zimmermann "Improving variable-fidelity surrogate modeling via gradient-enhanced kriging and a generalized hybrid bridge function." Aerospace Science and Technology 25.1 (2013): 177-189.

[41] Gary G. Wang, S. Shan "Review of metamodeling techniques in support of engineering design optimization." Journal of Mechanical Design 129.4 (2007): 370-380.

[42] Shinkyu Jeong, Mitsuhiro Murayama, Kazuomi Yamamoto "Efficient optimization design method using kriging model" Journal of aircraft 42.2 (2005): 413-420.

[43] Nestor V. Queipo, Javier V. Goicochea, Salvador Pintos. "Surrogate modeling-based optimization of SAGD processes." Journal of Petroleum Science and Engineering 35.1 (2002): 83-93.

[44] Hyoung-Seog Chung, Juan J. Alonso. "Using gradients to construct cokriging approximation models for high-dimensional design optimization problems." AIAA paper 317 (2002): 14-17.

[45] Songqing Shan, G. Gary Wang. "Survey of modeling and optimization strategies to solve high-dimensional design problems with computationally-expensive black-box functions." Structural and Multidisciplinary Optimization 41.2 (2010): 219-241.

[46] Jonas Sjberg et al. "Nonlinear black-box modeling in system identification: a unified overview." Automatica 31.12 (1995): 1691-1724.

[47] Laurens JP van der Maaten, Eric O. Postma, H. Jaap van den Herik "Dimensionality reduction: A comparative review." Journal of Machine Learning Research 10.1-41 (2009): 66-71.

[48] T.R. Browning "Applying the design structure matrix to system decomposition and integration problems: a review and new directions" IEEE Trans Eng Manage 48.3 (2001): 292-306

[49] Raymond H. Myers, Douglas C. Montgomery, Christine M. Anderson-Cook "Response surface methodology: process and product optimization using designed experiments" Vol. 705. John Wiley and Sons, 2009

[50] Ira H. Abbott, E. Albert Von Doenhoff "Theory of wing sections" Dover Publications Inc., Section 4.2 (1959)

[51] Tsan-Hsing Shih, et al. "A new k- eddy viscosity model for high reynolds number turbulent flows" Computers and Fluids 24.3 (1995): 227-238.

[52] Virendra C. Patel, Wolfgang Rodi, and Georg Scheuerer "Turbulence models for near-wall and low Reynolds number flows-a review" AIAA journal 23.9 (1985): 1308-1319

[53] Toby S. Cubitt, Jens Eisert, Michael M. Wolf "Extracting dynamical equations from experimental data is NP hard" Physical review letters 108.12 (2012): 120503

[54] Rick Salmon "Hamiltonian fluid mechanics" Annual review of fluid mechanics 20.1 (1988): 225-256

[55] Randall J. LaVeque "Finite volume methods for hyperbolic problems" Vol. 31. Cambridge university press, 2002

[56] Pieter Eykhoff "System identification, parameter and system estimation" John Wiley and Sons, 1974

[57] S.A. Billings, W.S.F Voon "Piecewise linear identification of non-linear system" International Journal of Control, 46.1 (1987): 215-235

[58] Georgios B. Giannakis, Erchin Serpedin "A bibliography on nonlinear system identification" Signal Processing 81.3 (2001): 533-580

[59] M.J. Korenberg, I.W. Hunter "The Identification of Nonlinear Biological Systems: Volterra Kernel Approaches" Annals Biomedical Engineering 24.2 (1996): 250-268

[60] Julian Jakob Bussgang "Crosscorrelation functions of amplitude-distorted Gaussian signals" (1952)

[61] C.P. Kwong, C. F. Chen "Linear feedback system identification via block-pulse functions" International Journal of Systems Science 12.5 (1981): 635-642

[62] S.A. Billings, I.J. Leontaritis "Identification of nonlinear systems using parametric estimation techniques" Proceedings of the IEE Conference on Control and its Application, Warwick, UK, pp.183-187

[63] Sheng Chen, S. A. Billings, P. M. Grant "Non-linear system identification using neural networks" International journal of control 51.6 (1990): 1191-1214

[64] Stephen A. Billings, Hua-Liang Wei "A new class of wavelet networks for nonlinear system identification." Neural Networks, IEEE Transactions on 16.4 (2005): 862-874.

[65] S. A. Billings, W. S. F. Voon "Correlation based model validity tests for non-linear models" International Journal of Control 44.1 (1986): 235-244.

[66] Tammo Jan. Dijkema "Adaptive tensor product wavelet methods for solving PDEs" PhD thesis, Utrecht University (2009)

[67] Ismail Kucuk, Ibrahim Sadek "An efficient computational method for the optimal control problem for the Burgers equation." Mathematical and computer modelling 44.11 (2006): 973-982.

[68] Qiqi Wang, Numpad package, https://github.com/qiqi/numpad.git

[69] Scikit-learn package, https://github.com/scikit-learn/scikit-learn.git

[70] Steven G. Johnson, The NLopt nonlinear-optimization package, http://ab-initio.mit.edu/nlopt

[71] John E. Dennis, Jorge J. Mor. "Quasi-Newton methods, motivation and theory." SIAM review 19.1 (1977): 46-89.

[72] Eric Alexander. Dow, "Quantification of structural uncertainties in RANS turbulence models." Dissertation, Massachusetts Institute of Technology, 2011.

[73] J. Nocedal. "Updating quasi-Newton matrices with limited storage" Mathematics of Computation, 35 (1980): 773-782

[74] Van der Maaten, Laurens JP, Eric O. Postma, and H. Jaap van den Herik. "Dimensionality reduction: A comparative review." Journal of Machine Learning Research 10.1-41 (2009): 66-71.

[75] Havi, Ron, and George H. John. "Wrappers for feature subset selection." Artificial intelligence 97.1 (1997): 273-324.

[76] Wei, Hua-Liang, and Stephen A. Billings. "Feature subset selection and ranking for data dimensionality reduction." Pattern Analysis and Machine Intelligence, IEEE Transactions on 29.1 (2007): 162-166.

[77] Jolliffe, Ian. Principal component analysis. John Wiley and Sons, Ltd, 2002.

[78] Gardner, Jacob, et al. "Bayesian optimization with inequality constraints." Proceedings of The 31st International Conference on Machine Learning. 2014.

[79] Tibshirani, Robert. "Regression shrinkage and selection via the lasso." Journal of the Royal Statistical Society. Series B (Methodological) (1996): 267-288.

[80] Dziak, John, Runze Li, and Linda Collins. "Critical review and comparison of variable selection procedures for linear regression (Technical report)." (2005).

[81] Derksen, Shelley, and H. J. Keselman. "Backward, forward and stepwise automated subset selection algorithms: Frequency of obtaining authentic and noise variables." British Journal of Mathematical and Statistical Psychology 45.2 (1992): 265-282.

[82] Zou, Hui, and Trevor Hastie. "Regularization and variable selection via the elastic net." Journal of the Royal Statistical Society: Series B (Statistical Methodology) 67.2 (2005): 301-320.

[83] Stone, Mervyn. "An asymptotic equivalence of choice of model by cross-validation and Akaike's criterion." Journal of the Royal Statistical Society. Series B (Methodological) (1977): 44-47.

[84] Schwarz, Gideon. "Estimating the dimension of a model." The annals of statistics 6.2 (1978): 461-464.

[85] J Mockus, V Tiesis, and A Zilinskas "The application of Bayesian methods for seeking the extreme." Towards Global Optimization, 2 (1978): 117-129

[86] Choi, Seongim, Juan J. Alonso, and Ilan M. Kroo. "Two-level multifidelity design optimization studies for supersonic jets." Journal of Aircraft 46.3 (2009): 776-790.

[87]

[88] Robinson, T. D., et al. "Multifidelity optimization for variablecomplexity design." Proceedings of the 11th AIAA/ISSMO Multidisciplinary Analysis and Optimization Conference, Portsmouth, VA. 2006.

[89] Torczon, Virginia. "On the convergence of pattern search algorithms." SIAM Journal on optimization 7.1 (1997): 1-25.

[90] Booker, Andrew J., et al. "A rigorous framework for optimization of expensive functions by surrogates." Structural optimization 17.1 (1999): 1-13.

[91] Andrew I. March "Multifidelity methods for multidisciplinary system design" Dissertation, Massachusetts Institute of Technology (2012)

[92] Aronszajn, Nachman. "Theory of reproducing kernels." Transactions of the American mathematical society (1950): 337-404.

[93] Meneveau, Charles, and P. Sagaut. Large eddy simulation for incompressible flows: an introduction. Springer Science and Business Media, 2006.

[94] Smagorinsky, Joseph. "General circulation experiments with the primitive equations: I. the basic experiment." Monthly weather review 91.3 (1963): 99-164.

[95] Moin, Parviz, and Krishnan Mahesh. "Direct numerical simulation: a tool in turbulence research." Annual review of fluid mechanics 30.1 (1998): 539-578.

[96] Li, Wu, Luc Hyuse, and Sharon Padula. "Robust airfoil optimization to achieve consistent drag reduction over a Mach range." No. ICASE-TR-2001-22. INSTITUTE FOR COMPUTER APPLICATIONS IN SCIENCE AND ENGINEERING HAMPTON VA, 2001.

[97] Verstraete, Tom, et al. "Optimization of a U-Bend for Minimal Pressure Loss in Internal Cooling ChannelsPart I: Numerical Method." Journal of Turbomachinery 135.5 (2013): 051015.

[98] Coletti, Filippo, et al. "Optimization of a U-Bend for Minimal Pressure Loss in Internal Cooling ChannelsPart II: Experimental Validation." Journal of Turbomachinery 135.5 (2013): 051016.

[99] Aimo Torn, Antanas Zilinskas "Global Optimization" Springer-Verlag New York, Inc. New York, NY, (1989)